Energy Conversion and Management 172 (2018) 138–154

Contents lists available at ScienceDirect

Energy Conversion and Management

journal homepage: www.elsevier.com/locate/enconman

Connected-top-bottom-cycle to cascade utilize flue gas heat for supercritical carbon dioxide coal fired power plant

Enhui Sun[a], Jinliang Xu[a,*], Mingjia Li[b], Guanglin Liu[a], Bingguo Zhu[a]

[a] Beijing Key Laboratory of Multiphase Flow and Heat Transfer for Low Grade Energy Utilization, North China Electric Power University, Beijing 102206, China
[b] Key Laboratory of Thermo-Fluid Science and Engineering of Ministry of Education, School of Energy & Power Engineering, Xi'an Jiaotong University, Xi'an, Shaanxi 710049, China

ARTICLE INFO

Keywords:
S–CO_2
Flue gas heat
Thermodynamic cycle
Heat transfer
Pressure drop

ABSTRACT

For coal fired power plant, the supercritical carbon dioxide Brayton cycle (S-CO_2) is difficult to absorb flue gas heat in a wide temperature range of 120–1500 °C. Here, novel methods are developed to cascade utilize flue gas heat, in which energies in high, moderate and low temperature levels are extracted by top cycle, bottom cycle or flue gas cooler (FGC), and air preheater, respectively. The cascade utilization shall satisfy the criterion that *CO_2 temperature entering boiler for top cycle equals to CO_2 temperature leaving boiler for bottom cycle*. The separate-top-bottom-cycle (STB) is proposed, in which no any component is shared by top and bottom cycles. Six possible bottom cycles are studied. The thermodynamics analysis is coupled with heat transfer and pressure drop analysis for whole power plant. It is found that the main vapor pressure of bottom cycle can be the "best" parameter to be adjusted over a wide range of 15–35 MPa to couple and optimize top and bottom cycles. Then, the *parameter coordination principle* is proposed to share specific components for top and bottom cycles. Thus, the separate cycles are converted into a connected cycle to simplify the whole system layout. The connected cycle has a power generation efficiency of 51.82% at main vapor parameters of 700 °C/35 MPa, significantly higher than available supercritical water-steam Rankine cycle power plant. The findings in this paper give a clue to further raise the power generation efficiency for large scale S-CO_2 coal fired power plant.

1. Introduction

High pressure water-steam Rankine cycle has been used for large scale power generation for more than one century, since the first coal fired power plant was put into operation in 1882 [1]. At the moment, the power generation efficiency is about 47% for large scale (~1000 MW) supercritical water-steam Rankine cycle power plant [2]. The classical thermodynamics tells us that the system efficiency can be further increased by increasing vapor temperature entering turbine. However, such improvement is restricted by temperature tolerance limit of materials. For example, the chemical reaction between water-steam and solid materials is enhanced at ultra-high temperature such as 700 °C, introducing the difficulty to further explore efficiency potential [3].

Scientists and engineers are searching new technologies for compact power systems. It is known that renewable energy such as wind energy or solar energy are unstable. When these energies are connected with a power grid, the power grid becomes fragile [4]. An effective way to create robust power grid is to develop hybrid power systems including renewable energy and coal fired power plant [5]. The coal fired power plant should have the capability to adjust power load at a fast speed. The coal fired power plant should be designed in a compact way to have small thermal inertia. Fundamentally, a water-steam Rankine cycle system is difficult to satisfy this requirement, because some components such as condenser operate in a vacuum pressure such as ~6 kPa [6] to cause low fluid density and large component size. Distributed energy utilization also demands smart and compact power systems [7,8].

Supercritical carbon dioxide Brayton cycle (called S-CO_2 cycle here) offers benefits to breakthrough above limitations. First, the thermal efficiency of a S-CO_2 cycle can be higher than a supercritical water-steam Rankine cycle [9]. Second, CO_2 is an inertia fluid to yield the weak chemical reaction between high temperature CO_2 and solid material [10], making it possible to further raise vapor temperature entering turbine. Third, S-CO_2 is a Brayton cycle to operate the whole system in high pressures such as > 7.38 MPa, resulting in high fluid densities to significantly reduce component sizes of turbines and coolers [11,12].

Sulzer [13] was the first to propose S-CO_2 cycle, which was

* Corresponding author.
E-mail address: xjl@ncepu.edu.cn (J. Xu).

https://doi.org/10.1016/j.enconman.2018.07.017
Received 16 April 2018; Received in revised form 13 June 2018; Accepted 6 July 2018

Nomenclature

C	compressor
CTB	connected-top-bottom-cycle
d	inside tube diameter, mm
DRH	double reheating
f	frictional coefficient
FGC	flue gas cooler
g	gravity acceleration
G	mass flux in a single tube, kg/m^2 s
h	specific enthalpy, kJ/kg
HTR	high temperature recuperator
l	tube length, m
LTR	low temperature recuperator
m	mass flow rate, kg/s
n	the number of tubes
N	number of flow length segments
P	pressure, MPa
PACC	partial cooling cycle
PRCC	pre-compression cycle
PH	preheater
Q	heat transfer rate, MW
RC	recompression cycle
Re	Reynolds number
RH	reheating
S-CO_2	supercritical carbon dioxide
SEC	split expansion cycle
SH	superheater
SHC	split heating cycle
SRC	simple recuperated cycle
STB	separate-top-bottom-cycle
T	turbine
T	temperature, ˚C
TTH	thermodynamic-thermal-hydraulic
u	flow velocity, m/s
x_{abs}	CO_2 flow rate split ratio
α_{ex}	excess air ratio

Subscripts

1, 2, 3…	state points of top cycle
1b, 2b, 3b…	state points of bottom cycle
abs	absorb
AP	air preheater
b	boiler
c	critical
e	electric
ex	exhaust
f	friction
fg	flue gas
i	in
LHV	lower heating value
o	out
p	pinch
s	isentropic
sec	secondary

Greek symbols

ρ	density, kg/m^3
ΔP	pressure drop
η_{th}	thermal efficiency
η_b	boiler efficiency
η_e	power generation efficiency
$\eta_{th,b}$	bottom cycle thermal efficiency
θ	inclination angle

analyzed by Feher [14]. The “Feher cycle” has been called in literature. Great attention has been paid on S-CO_2 cycle in recent years. Most of studies have been focused on S-CO_2 cycles driven by nuclear energy [15–17], solar energy [18–20], or waste heat from gas turbine [21–23], including thermodynamics analysis [18,24,25], heat transfer characteristics [26–28] and small-scale component demonstration [29–31]. Because we deal with S-CO_2 coal fired power plant, S-CO_2 nuclear, solar or gas turbine power plants are not commented one by one here.

When S-CO_2 cycle is used for coal fired power plant, the thermal coupling between boiler and cycle is a major issue. S-CO_2 coal fired power plant is in concept design stage. Moullec [32] and Mecheri et al. [33] noted higher thermal efficiency of S-CO_2 cycle compared with water-steam Rankine cycle, even considering post-combustion carbon capture process (CCS) [32,34,35].

For a similar power capacity, the CO_2 mass flow rate shall be several times of a water-steam Rankine cycle [32,36]. The boiler pressure drop becomes ultra-large if a conventional boiler design is used, which is the first challenge to be overcome. The second challenge is how to recover residual flue gas heat in boiler tail flue. In a boiler, the flue gas temperature covers a wide range from 120 ˚C to 1500 ˚C, in which the ~120 ˚C limit is specified by the finally discharged flue gas temperature. A single S-CO_2 cycle cannot absorb heat from heat source in such a wide temperature range. Usually, an air preheater is installed in boiler tail flue to absorb part of residual flue gas heat. When the amount of residual heat is large, using air preheater alone not only introduces an ultra-large air preheater size, because the heat transfer coefficients of both air and flue gas are small, but also causes safety issue for power plant, because the high temperature air may cause “explosive burning” in furnace [37]. Some researchers [32,33,38–40] added an additional heat exchanger called flue gas cooler (FGC) in boiler tail flue to absorb part of residual flue gas heat. A CO_2 flow stream is extracted from total CO_2 flow rate at the outlet of main or auxiliary compressor. Then, the CO_2 stream after being heated by FGC is returned to S-CO_2 cycle. This method can be called the FGC method.

Because the outlet flue gas temperature discharged to environment is decreased by using FGC, the boiler efficiency is increased. However, because an additional heat is added to the cycle, the cycle thermal efficiency is decreased. We note that the power generation efficiency is the outcome of cycle thermal efficiency and boiler efficiency. There is a tradeoff between boiler efficiency and cycle thermal efficiency. Here, the FGC method is revisited, it is found that there exists the efficiency potential to be explored. One may ask a question that if it is possible to maximize both the cycle thermal efficiency and the boiler efficiency simultaneously. Inspired by this question, the “*three/four temperature regimes*” is proposed for cascade utilization of flus gas energy over full temperature range. The top cycle, bottom cycle and air preheater absorb flue gas heat in high, moderate and low temperature regime, respectively. Thus, the separate-top-bottom-cycle is established. A specific running parameter is carefully selected so that it can be varied over a wider range but has less effect on cycle performance. Thus, the total flue gas energy is reasonably distributed among top cycle, bottom cycle and air preheater to ensure better performance of both the top and bottom cycles. Finally, the “*parameter coordination principle*” is proposed to combine the two cycles into one to simplify the whole system design. Our results show that the connected-top-bottom-cycle (CTB) apparently improves performance compared with supercritical water-steam Rankine cycle power plant.

This paper is organized as follows. Section 2 describes the cycles for cascade utilization of flue gas energy, including RC + DRH + FGC (recompression cycle + double reheating + FGC) shown in Section 2.1

for method 1 (see Figs. 1 and 2), STB (separate-top-bottom-cycle) shown in Section 2.2 for method 2 (see Figs. 3–12), and CTB (connected-top-bottom-cycle) shown in Section 2.3 for method 3 (see Figs. 13–15). Section 3 deals with the numerical methods for coupling calculations of boiler and thermodynamic cycle, including Section 3.1 for cycle computation, Section 3.2 for thermal-hydraulic computation, and Section 3.3 for energy distribution computation. Section 4 is for results and discussion corresponding to the three methods of flue gas heat absorption, containing Section 4.1 for the outcome of RC + DRH + FGC, Section 4.2 for the outcome of STB, and Section 4.3 for the outcome of CTB. The conclusions are summarized in Section 5.

2. Cascade utilization of flue gas heat over entire temperature range

In this section, we explain the fundamental cascade utilization principle for flue gas heat absorption over entire temperature range. Then, the three types of cycles are described corresponding to three methods of flue gas energy utilization. For all the three methods, an air preheater is included to recover low temperature flue gas energy. The three methods satisfy the *energy cascade utilization* principle.

For method 1 (see Fig. 1):

$$Q_{\text{flue gas}} = Q_{\text{heaters 1, 2, 3}} + Q_{\text{FGC}} + Q_{\text{AP}} \quad (1)$$

For methods 2 and 3 without FGC (see Figs. 3, 10, 11 and 12):

$$Q_{\text{flue gas}} = Q_{\text{heaters 1, 2, 3 for top cycle}} + Q_{\text{heater 4 for bottom cycle}} + Q_{\text{AP}} \quad (2)$$

For method 3 with FGC (see Figs. 13 and 14):

$$Q_{\text{flue gas}} = Q_{\text{heaters 1, 2, 3 for top cycle}} + Q_{\text{heater 4 for bottom cycle}} + Q_{\text{FGC}} + Q_{\text{AP}} \quad (3)$$

where $Q_{\text{flue gas}}$, $Q_{\text{heaters 1,2,3}}$, $Q_{\text{heater 4}}$, Q_{FGC} and Q_{AP} are total available flue gas energy received by thermal system, amount of heat received by heaters 1, 2 and 3, by heater 4, by FGC, and by air preheater, respectively. It is seen that three or four temperature regimes are set to fulfill the energy cascade utilization principle. Heat transfer components are consecutively arranged along a temperature decrease direction. In such a way, the flue gas energy is thoroughly utilized over a wide temperature range. The energy cascade utilization principle satisfies the criterion that the CO_2 temperature entering boiler for top cycle equals to the CO_2 temperature leaving boiler for bottom cycle. Practically, T_4

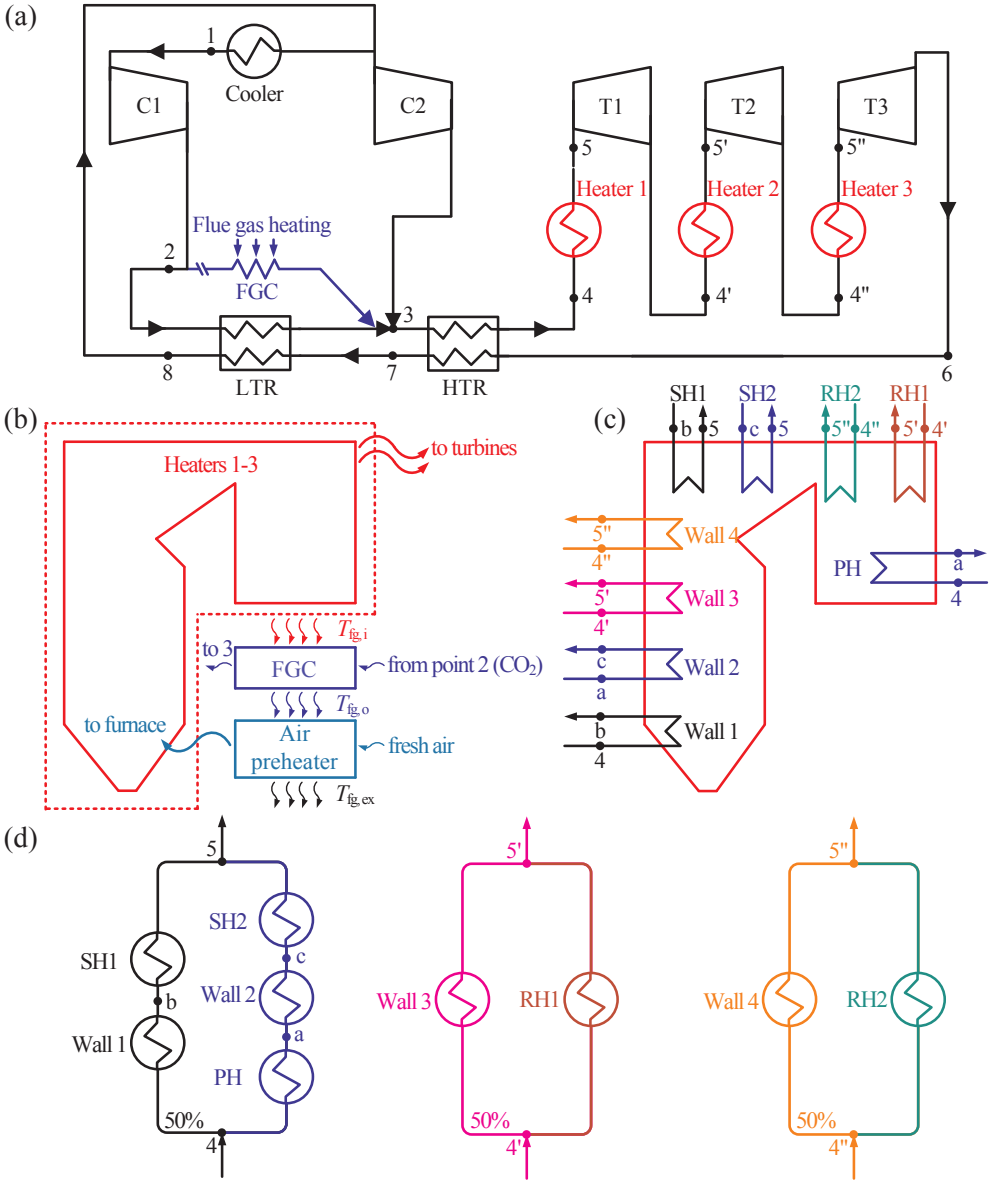

Fig. 1. RC + DRH + FGC to extract flue gas heat (a: the cycle; b: cascade utilization of flue gas heat; c: boiler module design; d: half flow strategy for heaters 1, 2 and 3).

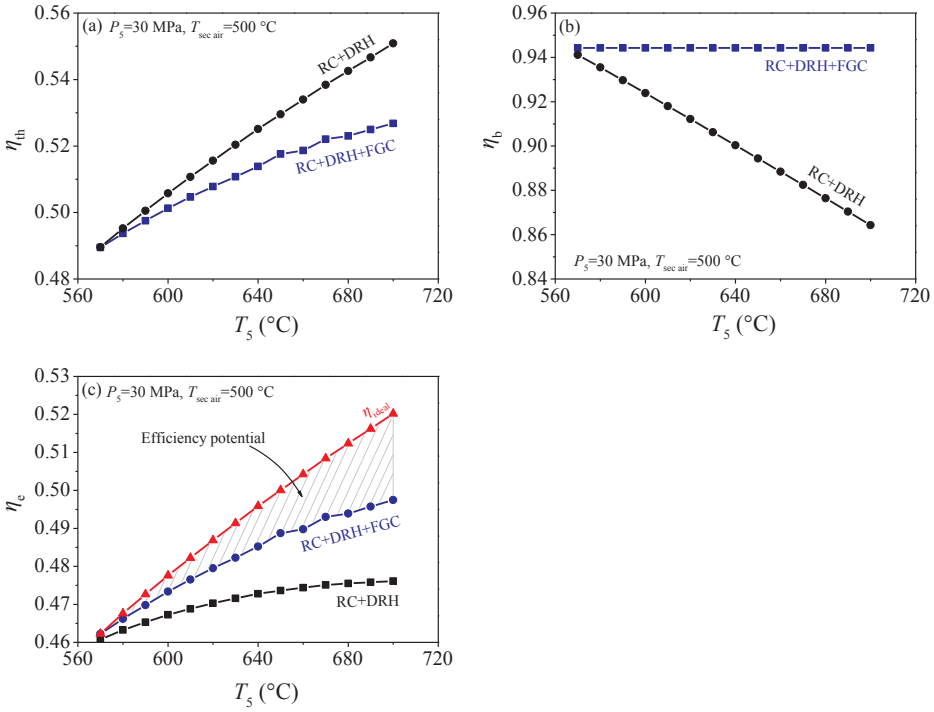

Fig. 2. Effect of FGC on cycle thermal efficiency and power generation efficiency (a: thermal efficiencies; b: boiler efficiencies; c: power generation efficiency potential).

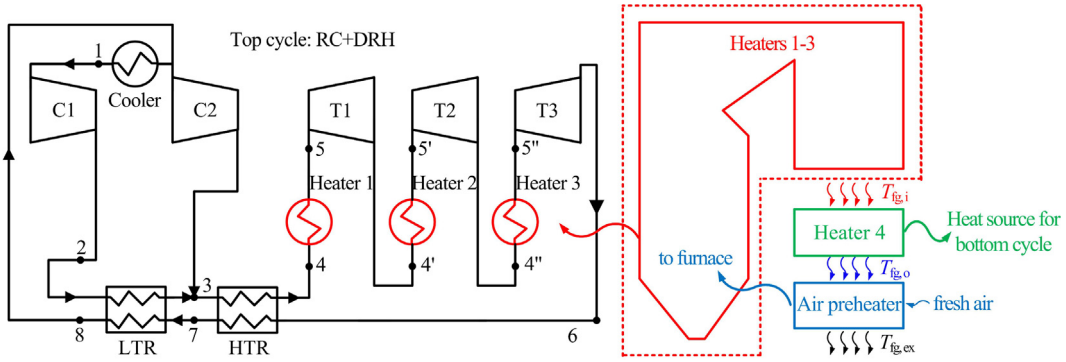

Fig. 3. cascade utilization of flue gas heat by separate-top-bottom-cycle (STB).

entering CO_2 preheater (PH) for top cycle equals to T_{5b} after being heated by heater 4 for bottom cycle, $T_4 = T_{5b}$ (see Figs. 3 and 4). Now we describe the three types of cycles corresponding to the three cascade utilization methods for flue gas energy extraction.

2.1. RC + DRH + FGC for method 1

Fig. 1a shows RC + DRH + FGC to recover flue gas energy. Recompression (RC) is a basic CO_2 cycle, which has been used in previous studies [41,42]. If FGC is removed from Fig. 1a, the cycle turns into recompression cycle with double reheating. The total CO_2 flow rate after low temperature recuperator heat exchanger (LTR) at point 8 is separated into two streams, with one stream flowing through a cooler, a main compressor (C1) and LTR, and the other line flowing through an auxiliary compressor (C2). Then the two streams are mixed at point 3 and enter the high temperature recuperator heat exchanger (HTR). Then, the mixed flow stream is heated by heater 1 and drives turbine 1 (T1) for power generation. The exhaust CO_2 stream after T1 is reheated by heater 2 and drives turbine 2 (T2) for power generation. Similar process is repeated by heater 3 and drives turbine 3 (T3). DRH ensures CO_2 vapor expansion in three turbines in a similar temperature level to improve the cycle efficiency. IF an FGC is involved in the system, a part of CO_2 flow rate is extracted from the outlet of C1 at point 2 and absorbs part of residual flue gas heat. Then, the extracted CO_2 flow rate enters HTR at point 3.

Method 1 divides the flue gas energy into three temperature levels (see Fig. 1b). Heaters 1, 2 and 3 are in high temperature regime. In this regime, heat transfer components consist of cooling walls 1–4, superheaters 1–2, reheaters 1–2, and CO_2 preheater (PH) (see Fig. 1c). It is known that CO_2 mass flow rate is much higher than that of a water-steam Rankine cycle, yielding non-acceptable boiler pressure drop. To overcome this difficulty, we introduce the *partial flow strategy* to ensure only half of the cycling flow rate flowing in each heat transfer component. If one keeps identical enthalpy increment for partial flow strategy and total flow strategy, heat transfer length can also be cut to be half. The simple analysis indicates that the friction pressure drop ΔP_f is scaled by m^3, where m is the mass flow rate. Thus, the partial flow strategy reduces friction pressure drop according to 1/8 principle compared with the total flow rate strategy. Fig. 1c and d shows how to fulfill the partial flow strategy to boiler design. The heater 1 integrates wall 1, SH1, PH, wall 2 and SH2. The total flow rate is divided into two paths, with half flow rate flowing in each path. The heater 2 includes

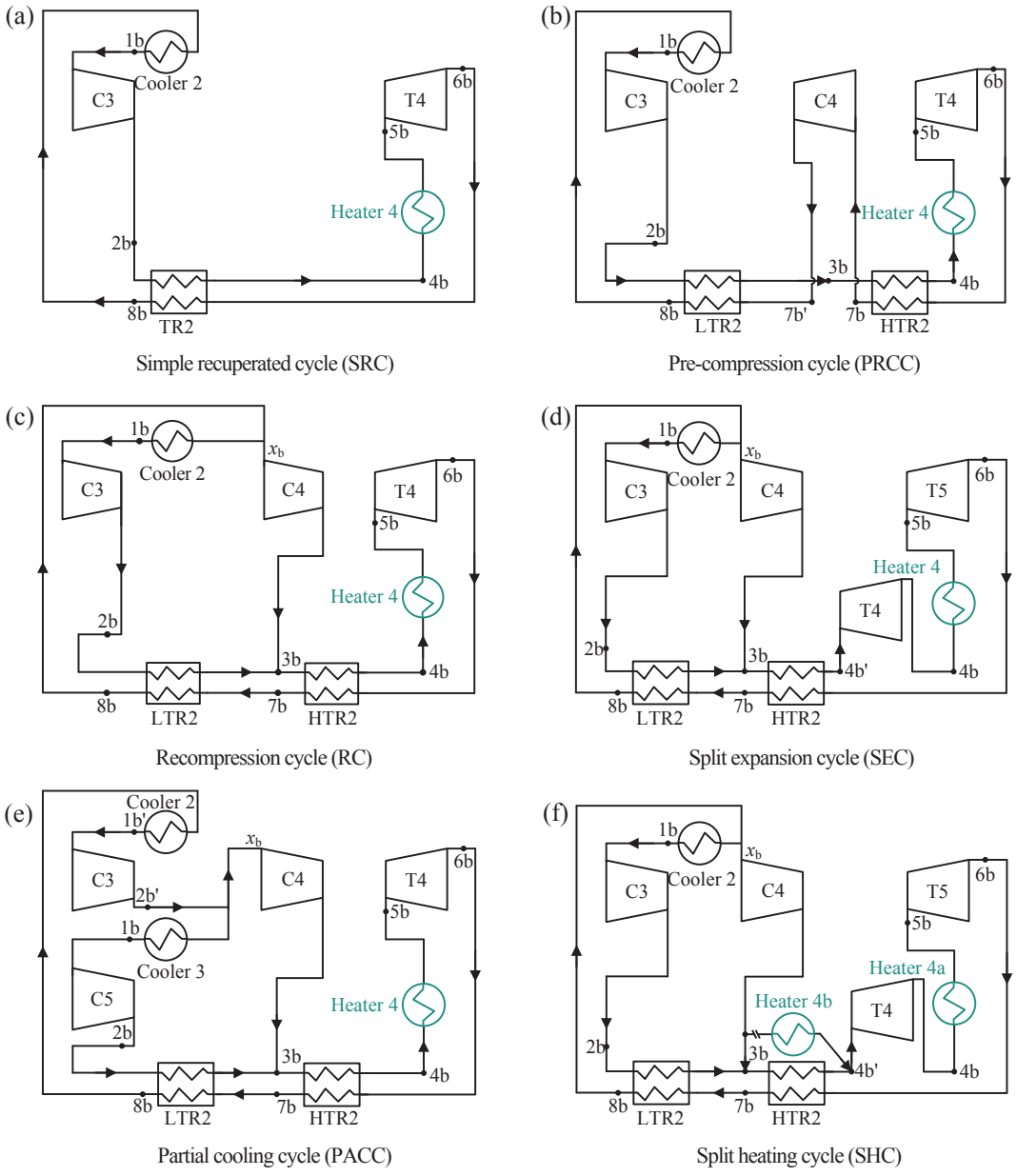

Fig. 4. Six possible bottom cycles that can be integrated with the whole thermal system.

wall 3 and RH1, with half flow rate flowing in each component. Similar arrangement is performed for the heater 3. The moderate temperature flue gas heat is recovered by FGC, and the low temperature flue gas heat is absorbed by air-preheater.

2.2. STB for method 2

Method 2 introduces a bottom cycle instead of FGC to recover moderate temperature flue gas energy. Heater 4 is the heat source to drive the bottom cycle. The top cycle still uses RC + DRH. Thus, we focus on the description of the bottom cycle (see Figs. 3 and 4). Six possible bottom cycles are described as follows:

Simple recuperated cycle (SRC, see Fig. 4a): It is a basic Brayton cycle including only one recuperator heat exchanger [43]. Along flow direction, the total CO_2 flow rate at point 4b is heated by heater 4 and drives turbine T4 for power generation. At the outlet of T4, the hot side CO_2 vapor dissipates heat to the cold side CO_2 fluid via TR2, then it is further cooled by cooler 2 and pressurized by compressor C3 to complete a cycle.

Pre-compression cycle (PRCC, see Fig. 4b): Compared with Fig. 4a, PRCC uses two recuperator heat exchangers instead of one. An additional compressor C4 is arranged in between the two recuperator heat exchangers. The cycle reaches subcritical state at the outlet of T4 [44]. Thus, the enthalpy difference across T4 is increased.

Recompression cycle (RC, see Fig. 4c): It is a typical RC, similar to Fig. 1a, except that there is only one heater involved.

Split expansion cycle (SEC, see Fig. 4d): SEC is extended from RC. CO_2 at the highest pressure point 4b'expands in turbine T4 first, then it is heated by heater 4. SEC reduces the temperature entering turbine T4 but increases the thermal load of recuperator heat exchangers.

Partial cooling cycle (PACC, see Fig. 4e): PACC can be considered as the combination of RC and PRCC, with the split flow characteristic similar to RC, and the trans-critical pressure characteristic similar to PRCC. The pressure P_{6b} at the outlet of turbine 4 (T4) is smaller than CO_2 critical pressure. Consecutively, the CO_2 fluid leaving T4 dissipates heat to the cold side of CO_2 via HTR2 and

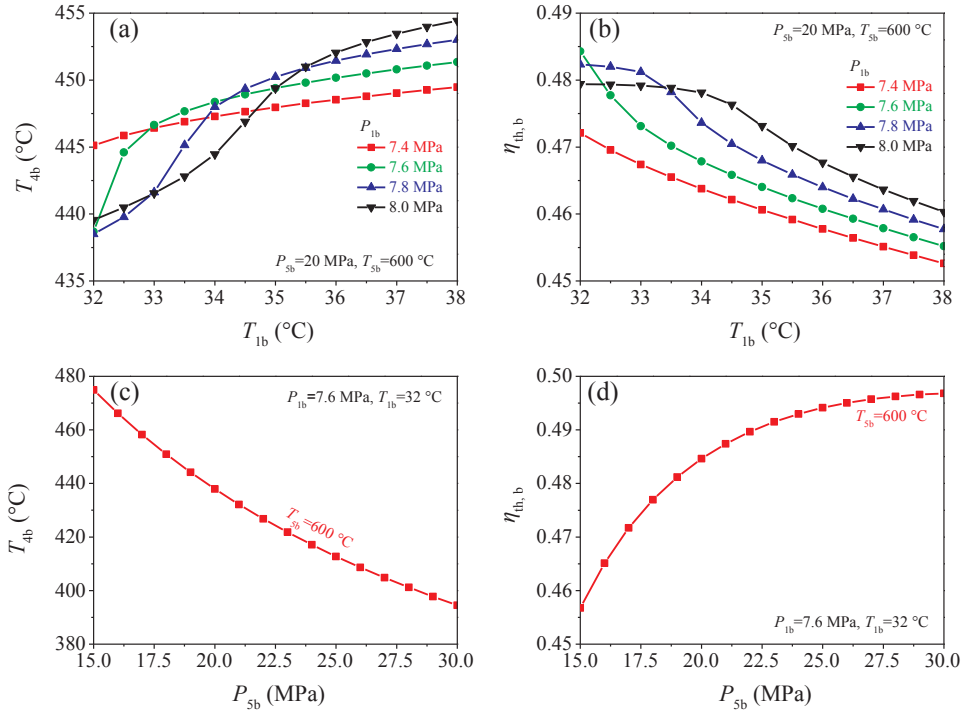

Fig. 5. Effect of cooler outlet temperatures T_{1b} and main vapor pressures P_{5b} on CO_2 temperatures entering heater 4 (T_{4b}) and bottom cycle thermal efficiencies $\eta_{th,b}$ for bottom cycle RC (see Fig. 4c).

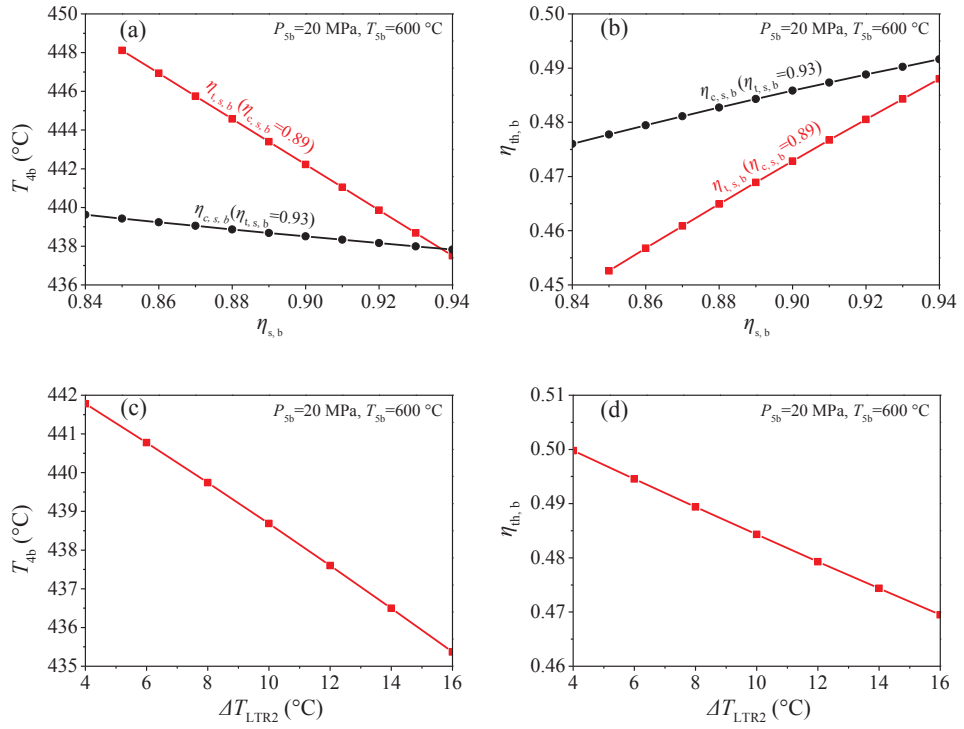

Fig. 6. Effect of isentropic efficiencies of compressor and turbine and pinch temperature differences of LTR2 on CO_2 temperatures entering heater 4 and bottom cycle efficiencies for bottom cycle RC.

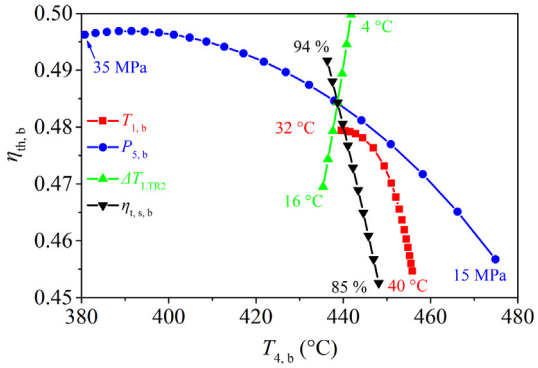

Fig. 7. Effect of various parameters on CO_2 temperatures entering heater 4 and bottom cycle efficiencies for RC bottom cycle.

LTR2, then is cooled by cooler 2 and re-compressed by C3 to supercritical state.

Split heating cycle (SHC, see Fig. 4f): SHC is our newly developed cycle in this paper, which is evolved from SEC. The difference between SHC and SEC is that SHC contains an additional heater in the cycle. Part of CO_2 flow rate is extracted from the auxiliary compressor (C4) outlet, heated by heater 4b and then enters the inlet of turbine T4. In such a way, the temperature at point 4b' is apparently increased. SHC has larger thermal efficiency than the cycles shown in Fig. 4a–e, except RC. SHC is suitable for cascade utilization of flue gas heat.

2.3. CTB for method 3

This section describes how to combine the top cycle and bottom cycle to form a simplified connected cycle. By comparing methods 1 and 2 for cascade utilization of flue gas energy, method 2 introduces additional bottom cycle. Thus, the number of cycle components is

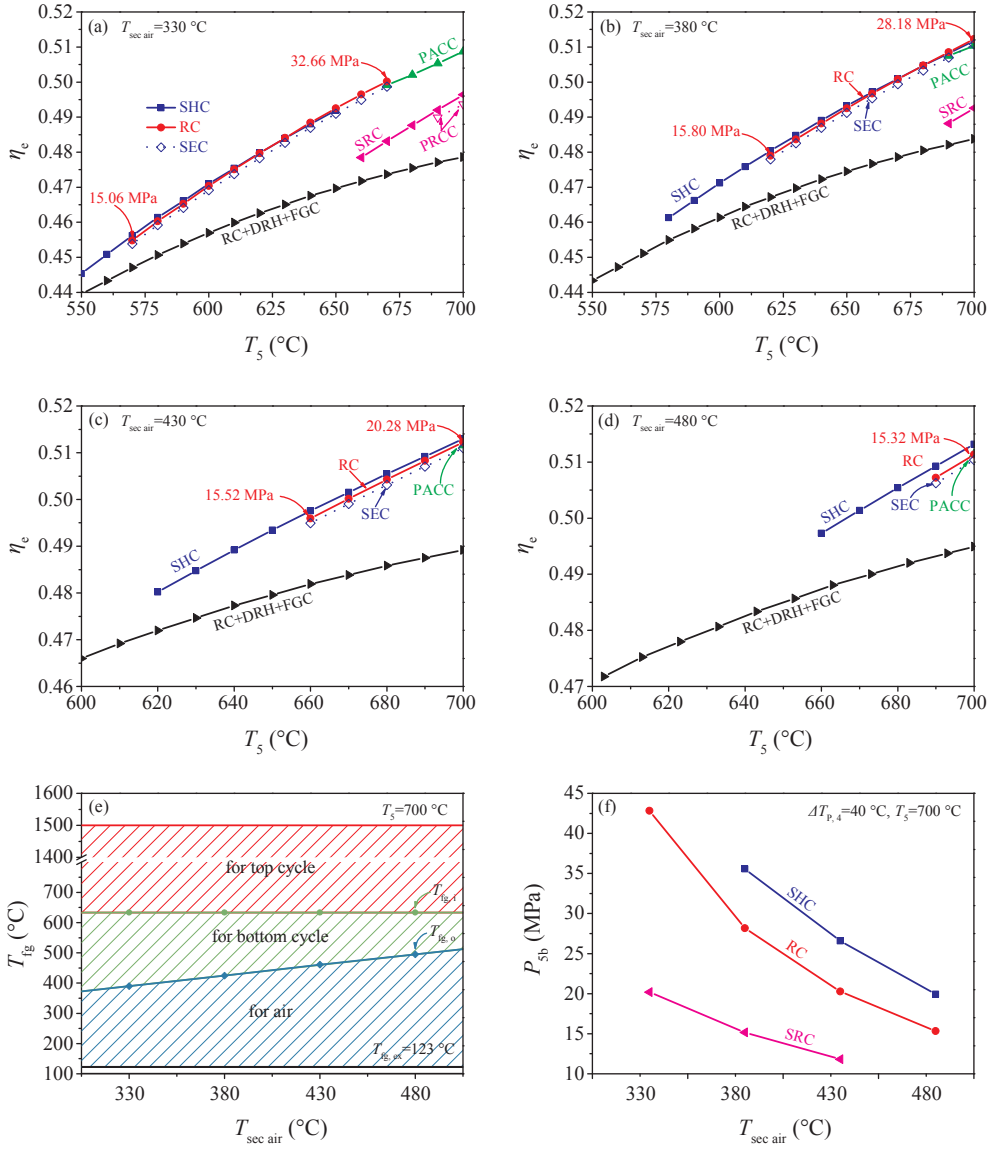

Fig. 8. Effect of secondary air temperatures $T_{sec\ air}$ and main vapor temperatures T_5 on power generation efficiencies and energy distribution in boilers ($\Delta T_{p,4}$ = 40 °C and P_5 = 30 MPa).

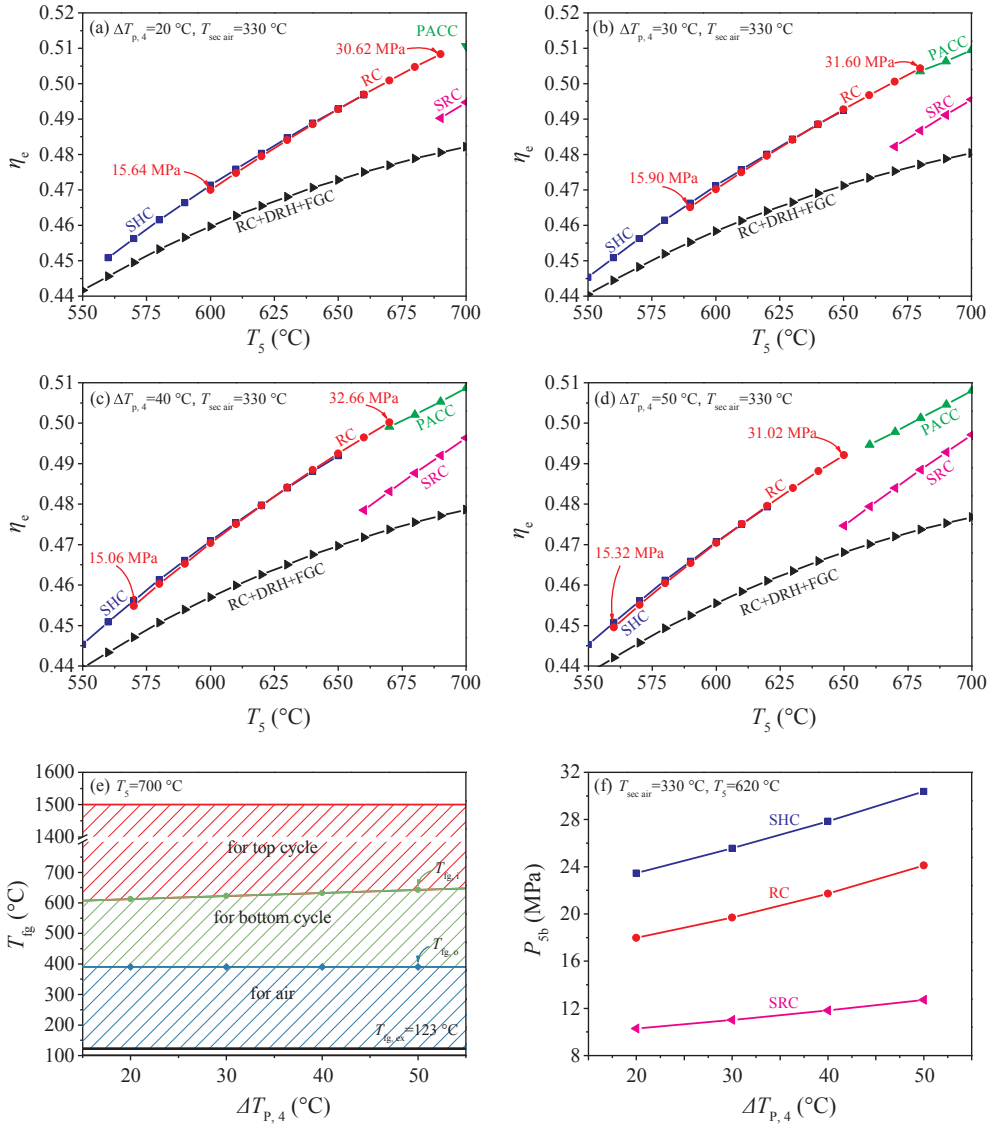

Fig. 9. Effect of $\Delta T_{p,4}$ and T_5 on power generation efficiencies and energy distribution in boilers (P_5 = 30 MPa).

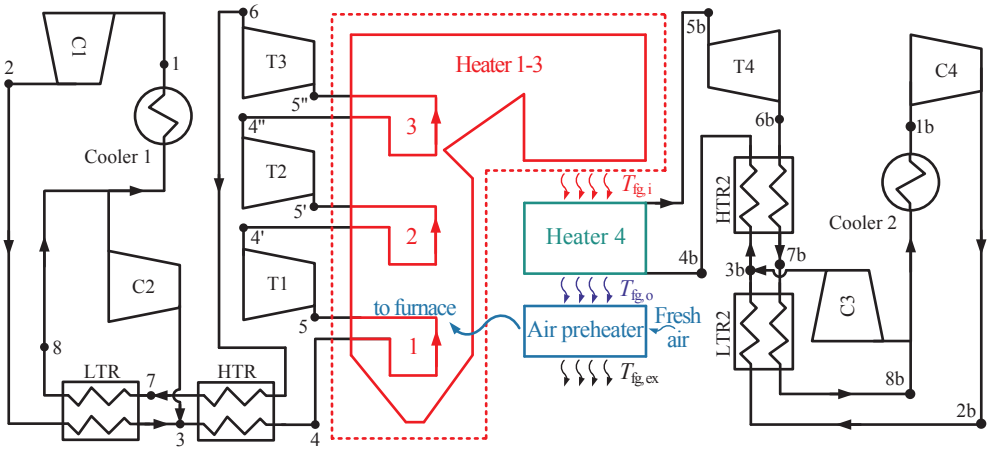

Fig. 10. The layout of STB(RC) with bottom cycle RC.

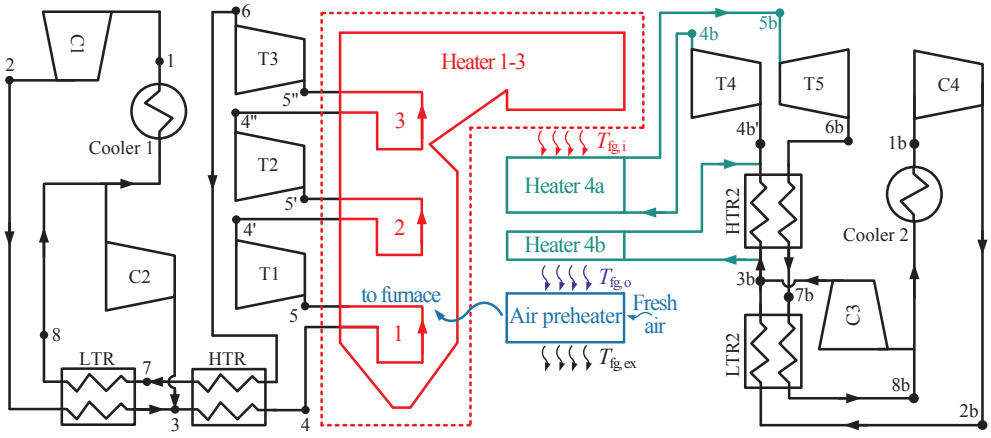

Fig. 11. The layout of STB(SHC) with bottom cycle SHC.

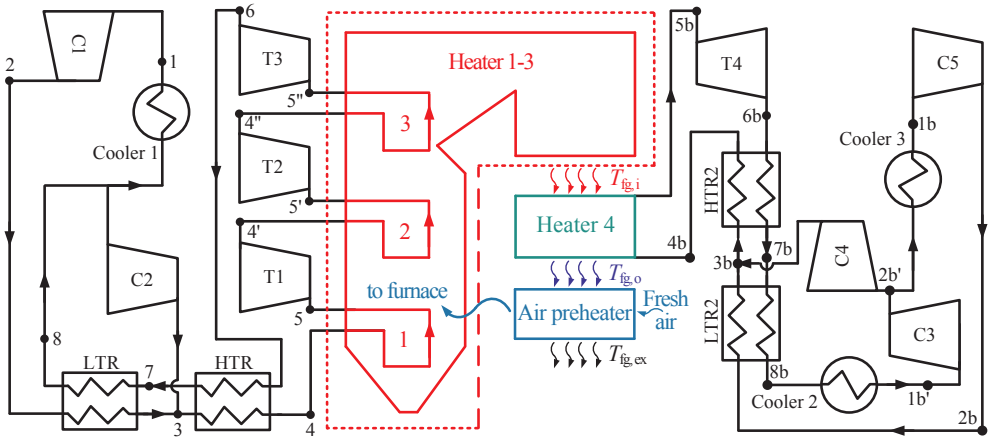

Fig. 12. The layout of STB(PACC) with bottom cycle PACC.

raised. One may ask that if it is possible to share specific components among the top and bottom cycles, but the overall system still keeps better performance. If one can do that, the two cycles can be connected to simplify the cycle layout. Fig. 10 shows the separate-top-bottom-cycle (STB) with the bottom cycle of RC, recorded as STB(RC). Alternatively, Fig. 13a shows the connected-top-bottom-cycle (CTB) with the bottom cycle of RC, recorded as CTB(RC). We examine how the separate cycles are converted into the connected cycle.

For cascade utilization of flue gas energy, even though the top cycle deals with high temperature flue gas energy, and the bottom cycle deals with moderate temperature flue gas energy, some components (not all) in the two cycles still have the possibility to share similar temperature/pressure values. Thus is the fundamental consideration to combine the two cycles together. Fig. 10 is revisited here. The left side and right side represent the top cycle and bottom cycle, respectively. Both cycles need a cooler (cooler 1 for top cycle, cooler 2 for bottom cycle) to dissipate heat to environment. Coolers 1 and 2 can have identical temperature/pressure values across the inlet and outlet. Thus, they can be combined into one. Similarly, the following groups of components can be combined into one: compressors C1 and C4, compressors C2 and C3, LTR and LTR2. Such simplification yields a single cycle layout shown in Fig. 13a. Generally, the black part represents “top” cycle, and the blue/green[1] part represent “bottom” cycle, but the two cycles are thoroughly mixed. The CO_2 flow rate at the outlet of the main compressor C1 splits into two paths, with one path flowing through LTR, HTR, the three groups of heaters and turbines consecutively, and the other path flowing through FGC, LTR2, heater 4 and turbine T4. In such a way, the number of components is reduced by four. Similar process is performed to convert STB(SHC) shown in Fig. 11 into CTB(SHC) shown in Fig. 14. The simplification process is called the *parameter coordination principle* in this paper.

3. Numerical methods

This section describes the cycle computation for the three types of methods for cascade utilization of flue gas energy. Our computation couples the thermodynamic cycle analysis and the boiler thermal-hydraulic characteristic. A thermodynamic-thermal-hydraulic code (called TTH) is developed in the authors' laboratory, consisting of a thermodynamics subroutine, a thermal-hydraulic subroutine and an energy distribution subroutine. The three subroutines are coupled to yield the S-CO_2 power plant design. As an appendix, Fig. A1 shows the logic framework of the code. There are two levels of iterations during the computation. The state parameter at any point includes CO_2 temperature and pressure. The pressure difference between two neighboring state points is pressure drop across a component, which should be calculated based on thermal load and component configuration. The CO_2 pressure distribution along the cycle is the first level of iteration. Initially, a reasonable CO_2 pressure distribution is assumed, but will be updated until a convergent solution is reached over the whole cycle.

The second level of iterations deals with the energy distribution among the thermodynamic cycle, FGC and air preheater, or among the top cycle, bottom cycle and air preheater. There are three intermediate

[1] For interpretation of color in Fig. 13, the reader is referred to the web version of this article.

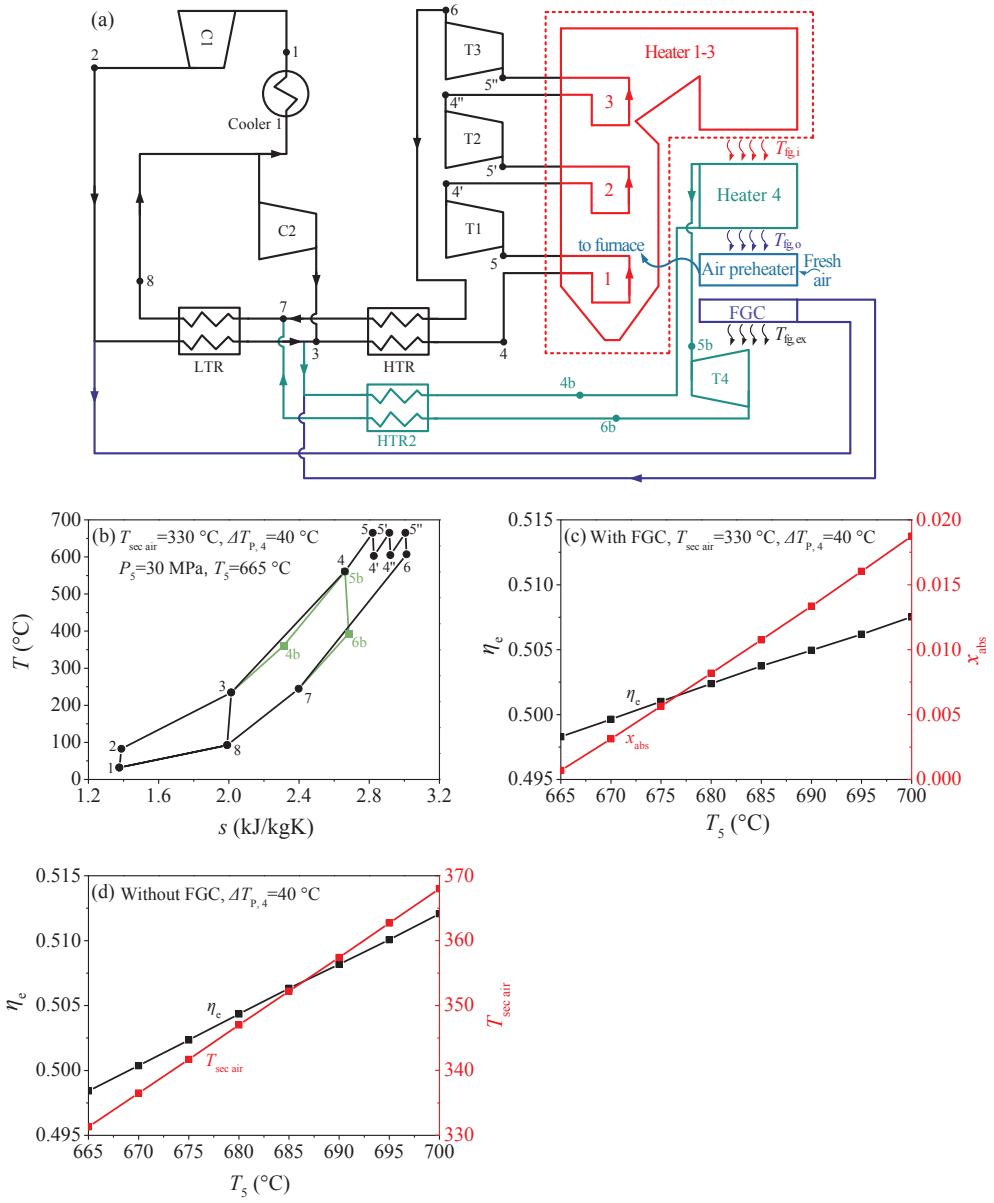

Fig. 13. CTB(RC) with bottom cycle RC and its overall performance (a: CTB(RC) layout; b: *T-s* diagram; c and d for power generation efficiencies with and without FGC).

temperatures: (1) $T_{fg,i}$: flue gas temperature at the interface between top cycle and FGC, or between top cycle and bottom cycle; (2) $T_{fg,o}$: flue gas temperature at the interface between FGC and air preheater, or between bottom cycle and air preheater; (3) $T_{fg\ ex}$: flue gas temperature discharged to environment. The three intermediate temperatures are coupled to determine the flue gas energy distribution (see Figs. 1 and 3). Initially, a reasonable energy distribution among top cycle and bottom cycle is calculated based on the state parameters at various points. By assuming the heat absorption of air preheater, the outlet temperature discharged to environment, $T_{fg\ ex}$, is determined. The calculation process is stopped until a convergent solution is reached to satisfy the requirement of $T_{fg\ ex}$ = 123 °C. We note that the intermediate temperatures $T_{fg,i}$ and $T_{fg,o}$ should be coupled with the CO_2 fluid temperatures by the following relationships:

$$T_{fg,i} = T_4 + \Delta T_{p,4} \quad (4)$$

$$T_{fg,o} = T_{4b} + \Delta T_{p,4b} \quad (5)$$

where T_4 is the CO_2 temperature entering CO_2 preheater for top cycle, T_{4b} is the CO_2 temperature entering heater 4 for bottom cycle, $\Delta T_{p,4}$ and $\Delta T_{p,4b}$ are the pinch temperature difference between flue gas and CO_2 at the corresponding points. In this paper, $\Delta T_{p,4b} = \Delta T_{p,4} - 10$ is assumed.

The computation has following assumptions: (1) steady operation of the system; (2) CO_2 physical properties coming from NIST software REFPROP [45]; (3) isentropic efficiencies for compressors of 0.89 [11,32,33] and for turbines of 0.93 [32,33,46], except that different values are used for sensitivity analysis; (4) pinch temperature of 10 K in recuperator heat exchangers of LTR and HTR; (5) convergent solution of identical temperatures/pressures of two fluid streams before mixing to minimize the exergy destruction; (6) heat loss of boiler considered but other heat losses neglected.

3.1. Thermodynamic cycle computation

The power plant design with a 1000 MWe net power output is our design target. Some important parameters should be specified at the beginning of the computation (see Table 1 for RC + DRH + FGC cycle,

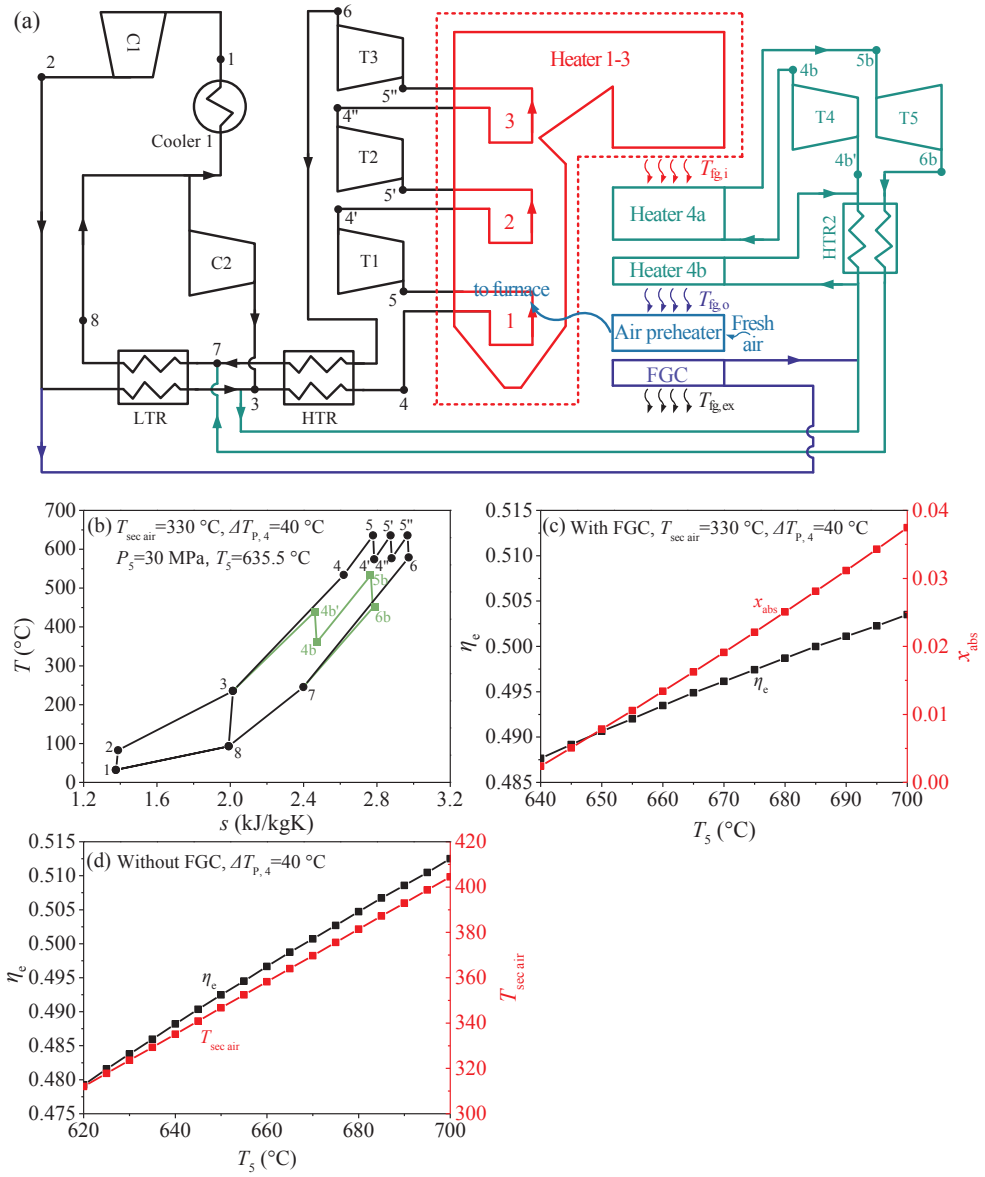

Fig. 14. CTB(SHC) with bottom cycle SHC and its overall performance (a: CTB(SHC) layout; b: *T-s* diagram; c and d for power generation efficiencies with and without FGC).

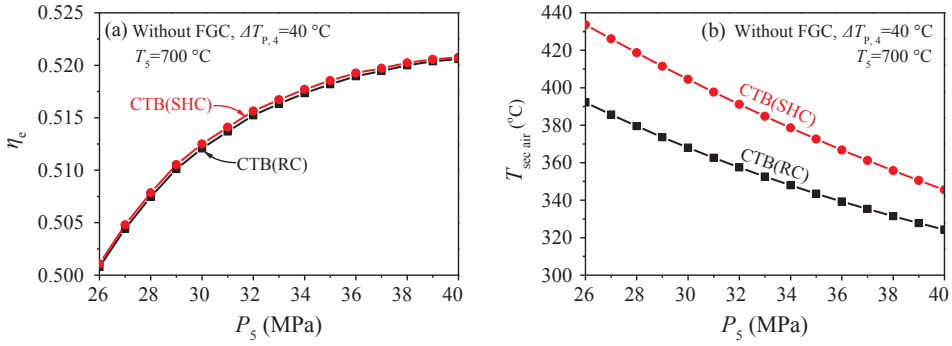

Fig. 15. Effect of main vapor pressures P_5 on power generation efficiencies and secondary air temperatures.

method 1 flue gas energy extraction). Methods 2 and 3 share similar input parameters. The main vapor parameters are T_5 (550–720 °C) and P_5 (30 MPa). The thermodynamics subroutine determines CO_2 temperatures and pressures at various state points. The total CO_2 mass flow rate m_{total} is

$$m_{total} = \frac{W_{net}}{w_{net}} \tag{6}$$

where W_{net} is the net power output which is targeted as W_{net} = 1000 MWe, w_{net} is the net power output per unit CO_2 mass flow

Table 1
Parameters for RC + DRH + FGC cycle considering boiler pressure drop and flue gas heat extraction.

Parameters	Values
Net power	1000 MW
Turbine inlet temperature (T_5)	550–720 °C
Turbine inlet pressure (P_5)	30 MPa
Turbine isentropic efficiency ($\eta_{t,s}$)	93%
Compressor C1 inlet temperature (T_1)	32 °C
Compressor C1 inlet pressure (P_1)	7.6 MPa
Compressors isentropic efficiency ($\eta_{c,s}$)	89%
Pressure drops in LTR and HTR (ΔP)	0.1 MPa
LTR and HTR pinch temperature difference (ΔT_{LTR} or ΔT_{HTR})	10 °C
Primary air temperature ($T_{pri\ air}$)	320 °C
Fresh air temperature entering air-preheater	31 °C
Ratio of primary air flow rate to the total air flow rate	19%
Secondary air temperature ($T_{sec\ air}$)	320–500 °C
Cold secondary air temperature	21 °C
Secondary air flow rate ratio	81%
Excess air coefficient (α_{ex})	1.2
Flue gas outlet temperature ($T_{fg,ex}$)	123 °C
Environment temperature	20 °C
Pinch temperature difference between flue gas and CO_2 in point 4 ($\Delta T_{p,4}$)	40 °C

rate. The power output for each turbine is determined by isentropic efficiency $\eta_{t,s}$ and enthalpy difference across the inlet and outlet. For turbine 1 (T1), the equations are

$$\eta_{t,s} = \frac{h_5 - h_{4'}}{h_5 - h_{4',s}}, \quad W_{t1} = m_{total}(h_5 - h_{4'}) \tag{7}$$

where $h_{4',s}$ is the enthalpy at point 4′ according to isentropic expansion. h_5, $h_{4'}$ are the enthalpy at points 5 and 4′, W_{t1} is the power output of T1. Other turbines share similar treatment.

The consumed work by compressor is treated as follows, for example for compressors C1 and C2:

$$\eta_{c,s} = \frac{h_{2,s} - h_1}{h_2 - h_1}, \quad W_{c1} = m_{c1}(h_2 - h_1) \tag{8}$$

$$\eta_{c,s} = \frac{h_{3,s} - h_8}{h_3 - h_8}, \quad W_{c2} = m_{c2}(h_3 - h_8) \tag{9}$$

where $h_{2,s}$ is the enthalpy at point 2 according to isentropic compression, h_1, h_2, h_3, h_8 are the enthalpy at points 1, 2, 3 and 8, respectively, W_c is the consumed work by compressor. Noting that m_{c1} is not equal to m_{total} due to flow split between C1 and C2, the criterion of $m_{total} = m_{c1} + m_{c2}$ should be satisfied.

The heat dissipated to environment is

$$Q_c = m_{c1}(h_8 - h_1) \tag{10}$$

The energy balance equations are written for LTR and HTR as

$$m_{LTR\ hot\ side}(h_7 - h_8) = m_{LTR\ cold\ side}(h_3 - h_2) \tag{11}$$

$$m_{HTR\ hot\ side}(h_6 - h_7) = m_{HTR\ cold\ side}(h_4 - h_3) \tag{12}$$

where h_4, h_6, h_7 are the enthalpy at points 4, 6 and 7, respectively, $m_{LTR\ hot\ side} = m_{HTR\ hot\ side} = m_{HTR\ cold\ side} = m_{total}$, $m_{LTR\ cold\ side} = m_{c1}$.

The thermal efficiency of thermodynamic cycle is

$$\eta_{th} = \frac{\sum W_t - \sum W_c}{Q_{flue\ gas} - Q_{AP}} \tag{13}$$

where ΣW_t is the total power output generated by all the turbines, ΣW_c is the total power consumed by all the compressors in the cycle.

3.2. Thermal-hydraulic computation

Our TTH code deals with the boiler thermal-hydraulic characteristic. Having the partial flow strategy, our calculation shows that the S-CO_2 boiler pressure drop is equivalent to, or even smaller than that of a supercritical water-steam Rankine cycle power plant. Fig. 1 shows the module design of various heat transfer components. The cooling walls 1, 2, 3 and 4 are radiative heat transfer surfaces. The superheaters 1, 2, reheaters 1, 2, and CO_2 preheater (PH) are convective heat transfer surfaces. Based on experience learned from large scale supercritical water-steam Rankine cycle power plant, cooling walls account for about half of the total boiler pressure drop. In order to simplify the computation, we assume

$$\Delta P = 2\Delta P_{f,\ cooling\ wall} + \Delta P_{g,\ cooling\ wall} \tag{14}$$

where ΔP, $\Delta P_{f,\ cooling\ wall}$ and $\Delta P_{g,\ cooling\ wall}$ are the boiler pressure drop, friction pressure drop of cooling wall, and gravity pressure drop of cooling wall, respectively.

The thermal-hydraulic subroutine contains thermal load distribution among various heat transfer modules. Once the module configuration parameters such as tube diameter, distance between neighboring tubes, and number of tubes are given, the pressure drop can be calculated. In order to consider the variation of CO_2 physical properties in terms of temperatures, a set of subsections are divided along the flow length of heat transfer module. The pressure drop is

$$\Delta P_{f,cooling\ wall} = \sum_{i=1}^{N} f_i \times \frac{\Delta l}{d_i} \times \frac{\rho_i u_i^2}{2} = \sum_{i=1}^{N} \frac{f_i G^2 \Delta l}{2\rho_i d_i} \tag{15}$$

$$\Delta P_{g,cooling\ wall} = \sum_{i=1}^{N} \rho_i g \Delta l \sin(\theta) \tag{16}$$

where N is the total number of segments along the flow length, d_i is the inside diameter of the tube, ρ_i is the CO_2 density, u_i is the flow velocity, G is the mass flux in a single tube, $\Delta l = l/N$, l is the tube length for a specific cooling wall module, θ is the inclination angle with respect to the horizontal position ($\theta = 23.578°$ for cooling walls 1 and 2, and $\theta = 90°$ for cooling walls 3 and 4). The friction factor f_i is cited from Ref. [47]:

$$f_i = \frac{1}{(1.82\lg(Re) - 1.64)^2} \tag{17}$$

where Re is the Reynolds number. The pressure drop computation is not sensitive to N if N is sufficiently large such as $N = 200$. A reasonable design yields $d_i = 40$ mm, $n = 1167$ for cooling walls 1 and 2 with inclined tubes, and $n = 2334$ for cooling walls 3 and 4 with vertical tubes, n is the number of tubes. Because radiative heat fluxes are large for modules 1 and 2, the inclined tubes of the two modules are useful to even the CO_2 vapor temperature distribution at the outlet. The boiler thermal-hydraulic calculation gives temperature/pressure distributions among various heat transfer components.

3.3. Energy distribution computation

The two intermediate temperatures of $T_{fg,i}$ and $T_{fg,o}$ determine the energy distribution in boiler. The relationship between flue gas temperatures and CO_2 temperatures at the two interfaces are decided by

Table 2
Properties of the designed coal.

C_{ar}	H_{ar}	O_{ar}	N_{ar}	S_{ar}	A_{ar}	M_{ar}	V_{daf}	$Q_{net,ar}$
61.70	3.67	8.56	1.12	0.60	8.80	15.55	34.73	23,442

C (carbon), H (hydrogen), O (oxygen), N (nitrogen), S (sulfur), A (ash), M (moisture), V (Volatile).
Subscripts ar, daf means as received, dry and ash free, $C_{ar} + H_{ar} + O_{ar} + N_{ar} + S_{ar} + A_{ar} + M_{ar} = 100$.
$Q_{net,ar}$ means low heat value of coal (kJ/kg).
Ratio of primary air flow rate to the total air flow rate: 19%.
Ratio of secondary air flow rate to the total air flow rate: 81%.

Eqs. (4) and (5). The amount of heat received by top cycle (Q_{top}), bottom cycle (Q_{bottom}) and air preheater (Q_{AP}) are

$$Q_{\text{heaters 1,2,3 for top cycle}} = m_{coal}(h_{T_{flame}} - h_{T_{fg,i}}) \tag{18}$$

$$Q_{\text{heater 4 for bottom cycle}} = m_{coal}(h_{T_{fg,i}} - h_{T_{fg,o}}) \tag{19}$$

$$Q_{AP} = m_{coal}(h_{T_{fg,o}} - h_{T_{fg,ex}}) \tag{20}$$

where h is the flue gas enthalpy, T_{flame} is the flame temperature, m_{coal} is the coal consumption rate (kg/s), which is calculated as

$$m_{coal} = \frac{Q_{top} + Q_{bottom}}{\eta_b Q_{LHV}} \tag{21}$$

where Q_{LHV} is the lower heating value of coal (Q_{LHV} = 23442 kJ/kg, see Table 2 for the design coal parameters), η_b is the boiler efficiency [37]:

$$\eta_b = 1 - \sum_{i=2}^{6} q_i/100 \tag{22}$$

where q_i is the heat loss. Heat losses due to incomplete chemical combustion (q_3), unburned carbon (q_4), furnace exterior heat transfer (q_5), and sensible heat of ash and slag (q_6), are $q_3 = 0$, $q_4 = 0.6$, $q_5 = 0.2$ and $q_6 = 0.06$, respectively. The heat loss due to exhaust gas (q_2) has the dominant contribution to the boiler efficiency, which is

$$q_2 = \frac{(h_{T_{fg,ex}} - \alpha_{ex} h_{air})(1 - q_4/100)}{Q_{LHV}} \times 100 \tag{23}$$

where α_{ex} is the excess air ratio, h_{air} is the cold air enthalpy entering the boiler. Holding the boiler efficiency, the power generation efficiency of power plant is $\eta_e = \eta_{th}\eta_b$.

4. Results and discussion

This section gives results for the three methods of flue gas energy extraction. Subsections 4.1, 4.2 and 4.3 are logically presented. Section 4.1 concludes that RC + DRH + FGC exists efficiency potential that is to be explored. Section 4.2 shows that indeed, STB apparently increases the power generation efficiency. Section 4.3 shows that even though CTB simplifies the cycle layout, it has similar performance as STB. In summary, CTB not only has simple cycle structure, but also has attracting thermal performance.

4.1. The outcome of RC + DRH + FGC

Fig. 1a shows RC + DRH + FGC. Classical thermodynamics tells us that the thermal efficiency can be improved by raising main vapor temperature entering turbine (T_5), relatively elevating CO_2 temperature entering boiler (T_4, CO_2 preheater PH in Fig. 1). For supercritical water-steam DRH cycle, T_4 is ~340 °C [48], but it is increased to about 510 °C for RC + DRH cycle. Similar phenomenon appears for the S-CO_2. We note that Eq. (4) gives the relationship between $T_{fg,i}$ and T_4. Because $T_{fg,i}$ determines the total amount of residual flue gas heat, the recovery of residual flue gas heat becomes difficult for RC + DRH.

FGC is expected to recover moderate temperature regime flue gas heat. Fig. 2 shows the effect of FGC on system performance. Because the heat absorbed by air preheater is fixed, the exhaust gas temperature limit $T_{fg,ex}$ = 123 °C may or may not be satisfied. It is noted the thermal efficiency is $\eta_{th} = W_{net}/Q_{\text{heaters 1,2,3}}$ without FGC, and $\eta_{th} = W_{net}/(Q_{\text{heaters 1,2,3}} + Q_{FGC})$ with FGC. Because an additional heat is added to cycle by FGC, RC + DRH + FGC lowers the thermal efficiency η_{th}, compared with that without FGC (see Fig. 2a). However, RC + DRH + FGC ensures higher boiler efficiency of η_b = 94.43% to satisfy the limit of $T_{fg,ex}$ = 123 °C (see Fig. 2b). On the other hand, the system without FGC significantly lowers the boiler efficiency, indicating that using air preheater alone is not sufficient to extract the flue gas heat to result in $T_{fg,ex} > 123$ °C.

Fig. 2c shows the power generation efficiencies (η_e). FGC apparently raises η_e with increases of main vapor temperatures (T_5). There is a tradeoff between thermal efficiency and boiler efficiency when FGC is involved. One may ask a question that if it is possible to raise both the two efficiencies simultaneously. An ideal power generation efficiency is the outcome of larger thermal efficiency without FGC and larger boiler efficiency with FGC. Inspired by this question, the hybrid cycle is explored which is described as follows.

4.2. The outcome of separate-top-bottom-cycle (STB)

The bottom cycle extracts moderate temperature flue gas heat to suppress the thermal load applied to air preheater and lower the exhaust gas temperature. The energy distribution among the heat received by top cycle, bottom cycle and air preheater dependents on the three intermediate temperatures (see Fig. 3):

$$\text{energy distribution} = f(T_{fg,i}, T_{fg,o}, T_{fg,ex}) \tag{24}$$

It is seen from Eqs. (4) and (5) that $T_{fg,i}$ and $T_{fg,o}$ are related to T_4, T_{4b} and $\Delta T_{p,4}$. Having the constraint of $T_{fg,ex}$ = 123 °C, Q_{AP} is determined by the secondary air temperature ($T_{sec\ air}$). Then, Eq. (24) is rewritten as

$$\text{energy distribution} = f(T_4, \Delta T_{p,4}, T_{sec\,air}, T_{4b}) \tag{25}$$

The saccade utilization principle ensures that the CO_2 temperature entering boiler for top cycle equals to the CO_2 temperature leaving boiler for bottom cycle: $T_4 = T_{5b}$. STB should satisfy following targets: (1) both top and bottom cycles have better thermal efficiencies; (2) higher boiler efficiency; (3) reasonable secondary air temperatures. For the item 1, the top cycle efficiency can be ensured due to higher temperature operation. Then, attention should be paid to keep better thermal efficiency of the bottom cycle. The item 2 can be ensured by setting $T_{fg,ex}$ = 123 °C. The item 3 can be ensured by reasonably allocating the energy distribution (see Eqs. (24) and (25). We note that the system performance is influenced by the thermal coupling between thermodynamic cycle parameters and flue gas parameters. Sections 4.2.1 and 4.2.2 deal with the effects of cycle parameters and flue gas parameters, respectively.

4.2.1. Effect of cycle parameters

Eq. (25) indicates the cycle parameters of T_4 and T_{4b}, and the flue gas parameters of $\Delta T_{p,4}$ and $T_{sec\ air}$. This section analyzes the effect of T_4 and T_{4b}. Based on the criterion that $T_4 = T_{5b}$, where T_{5b} is the highest temperature of the bottom cycle, attention is turned to the effect of T_{5b} and T_{4b}. The objective of this section is to search suitable adjustment parameters so that T_{4b} can be varied over a wider range and the bottom cycle efficiency is insensitive to such adjustment. Because T_{5b} does not influence the parameter selection process, attention is paid to T_{4b} with constant T_{5b} = 600 °C. For the bottom cycle, T_{4b} and $\eta_{th,b}$ are the functions of following parameters:

$$\begin{cases} T_{4b} = f(P_{5b}, T_{1b}, P_{1b}, \eta_{t,s,b}, \eta_{c,s,b}, \Delta T_{LTR2}, \Delta T_{HTR2}) \\ \eta_{th,b} = f(P_{5b}, T_{1b}, P_{1b}, \eta_{t,s,b}, \eta_{c,s,b}, \Delta T_{LTR2}, \Delta T_{HTR2}) \end{cases} \tag{26}$$

Table 3
The bottoming cycle parameters.

Variable/parameter	Value(s)
Turbine inlet temperature (T_{5b})	400–600 °C
Turbine inlet pressure (P_{5b})	15–35 MPa
Turbine isentropic efficiency ($\eta_{t,s}$)	93%
Compressor inlet temperature (T_{1b})	32 °C
LP compressor inlet pressure (P_{1b})	7.6 MPa
Compressors isentropic efficiency ($\eta_{c,s}$)	89%
Pressure drop of each component except the boiler (ΔP)	0.1 MPa
Pressure drop of the boiler (ΔP_b)	0.2 MPa
LTR and HTR pinch temperature difference (ΔT_{LTR2} or ΔT_{HTR2})	10 °C

where the subscript b means the bottom cycle, P_{5b} is the main vapor pressure, T_{1b} and P_{1b} are the temperature and pressure at cooler outlet, $\eta_{th,b}$ is the thermal efficiency of bottom cycle, $\eta_{t,s,b}$ and $\eta_{c,s,b}$ are the isentropic efficiencies of turbine and compressor respectively, ΔT_{HTR2} and ΔT_{LTR2} are pinch temperatures of HTR2 and LTR2 respectively (see Fig. 4). With $\Delta T_{HTR2} = \Delta T_{LTR2}$, only six parameters are involved to influence T_{4b} and $\eta_{th,b}$. For the sensitivity analysis, Table 3 lists some important parameters for the bottom cycle computation.

When a Brayton cycle operates compressor near the critical point, the compressor consumed work is smaller [11]. Cooler 2 of bottom cycle influences the CO_2 temperature at cooler outlet (T_{1b}). Fig. 5a and b shows that at $P_{1b} = 7.4$ MPa $\approx P_c$, when T_{1b} is varied in the range of 32–38 °C, T_{4b} and $\eta_{th,b}$ are changed in the ranges of 445.1–449.5 °C, and 47.21–45.26%, respectively, which are narrow. When P_{1b} deviates from P_c, the variation ranges of T_{4b} and $\eta_{th,b}$ are enlarged for the same T_{1b} variation range, but this is not expected because $P_{1b} \gg P_c$ raises the compressor work. Thus, T_{1b} is not a good adjustable parameter.

Fig. 5c and d shows the effect of main vapor pressure (P_{5b}) on T_{4b} and $\eta_{th,b}$. Responding to the P_{5b} variation range of 15–30 MPa, T_{4b} is varied in the range of 474.9–394.5 °C, which is acceptable for flexible operation. For bottom cycle, higher main vapor pressure decreases the CO_2 temperature entering heater 4 to reduce thermal load applied to air preheater. Besides, the thermal efficiencies $\eta_{th,b}$ are increased from 45.67% to 49.68% adapting the P_{5b} range of 15–30 MPa. Most importantly, a P_{5b} variation range of 25–30 MPa not only keeps higher $\eta_{th,b}$ of 49.41–49.68%, but also yields an acceptable T_{4b} variation range of 412.7–394.5 °C. We conclude P_{5b} as a perfect adjustment parameter.

Fig. 6a and b shows the effect of isentropic efficiencies of compressor ($\eta_{c,s,b}$) and turbine ($\eta_{t,s,b}$) on T_{4b} and $\eta_{th,b}$. For compressor, a $\eta_{c,s,b}$ variation range of 0.84–0.94 results in acceptable $\eta_{th,b}$ of 47.60–49.16%, but a narrow T_{4b} variation range of 1.8 °C. For turbine, when its efficiencies are changed from 0.85 to 0.94, T_{4b} is changed in a range of about 10 °C, but the cycle thermal efficiencies are lower. Fig. 6a and b shows that both isentropic efficiencies of compressor and turbine are not suitable to be the adjustment parameters. In fact, the isentropic efficiencies of the two components are relied on their design and cannot be changed too much during operation.

For S-CO_2 cycle, the turbine outlet still keeps higher CO_2 temperature. The two heat exchangers HTR2 and LTR2 dissipate heat from hot CO_2 side to cold CO_2 side, reducing the CO_2 temperature before entering cooler. The pinch temperatures of the two heat exchangers characterize the sufficient degree of heat transfer between hot side and cold side. A small pinch temperature demands a large heat transfer area. Fig. 6c and d illustrates the effect of pinch temperatures of HTR2 and LTR2 on T_{4b} and $\eta_{th,b}$. As pinch temperatures are increased from 4 °C to 16 °C, T_{4b} is varied in a range of 6.4 °C, but the thermal efficiency of bottom cycle is decreased from 49.98% to 46.95%, which is not acceptable. Thus, pinch temperatures of HTR2 and LTR2 cannot be the adjustment parameters.

Fig. 7 summarizes the effect of four parameters on T_{4b} and $\eta_{th,b}$. The adjustment parameter should obey the following criteria: (1) wider variation range of the adjustment parameter; (2) acceptable thermal efficiency of bottom cycle that is insensitive to the adjustment parameter variations; (3) suitable T_{4b} values, that ensures suitable thermal load applied to air preheater. Based on the above analysis, T_{1b}, ΔT_{LTR2} and $\eta_{t,s,b}$ not only create a narrower T_{4b} variation range, but also generate higher $T_{4b} > 435$ °C. Thus, they are not the suitable adjustment parameters. P_{5b} is the "best" adjustment parameter to satisfy the criteria. It is noted that for PACC, there are two cooler outlet temperatures $T_{1b'}$ and T_{1b}, $T_{1b'}$ is treated as the adjustment parameter instead of P_{5b}.

4.2.2. Effect of air and flue gas parameters

For STB, the CO_2 preheater (PH) couples flue gas temperature $T_{fg,i}$ and CO_2 temperature T_4 by Eq. (4), where $\Delta T_{p,4}$ characterizes the sufficient degree of heat transfer between flue gas and CO_2. Thus, $\Delta T_{p,4}$ is selected as a coupling parameter whose effect is to be explored. The air preheater is another facility that influences thermal load allocation among top cycle, bottom cycle and air preheater. Thus, the effect of secondary air temperature $T_{sec\ air}$ should be studied. Fig. 8 explores the effect of $T_{sec\ air}$ on STB at different main vapor temperatures T_5 (see Table 1 for power plant parameters). Four key points are identified based on Fig. 8a–d.

Higher hybrid cycle efficiency: At all $T_{sec\ air}$, the separate-top-bottom-cycle (STB) has higher power generation efficiencies than RC + DRH + FGC, demonstrating the benefit of bottom cycle instead of FGC. The efficiency difference between STB and RC + DRH + FGC is more obvious at higher main vapor temperatures T_5.

Suitable bottom cycles for different T_5 ranges: The hybrid cycles with bottom cycle of PACC, SRC and PRCC are suitable for higher T_5 with narrow T_5 range. More attention is paid to the hybrid cycles with bottom cycle of RC and SHC. At $T_{sec\ air}$ of 330 °C and 380 °C, the bottom cycles RC and SHC not only maintain higher power generation efficiencies, but also cover wide T_5 ranges. The T_5 ranges adapting the two bottom cycles are overlapped, RC and SHC are more suitable for higher T_5 regime and lower T_5 regime, respectively. At higher $T_{sec\ air} = 430$ °C, RC is only satiable for higher T_5, whose range is relative narrow. SHC adapts a wider T_5 range from 620 °C to 700 °C. For lower T_5 such as 620 °C, SHC can only be used for bottom cycle. SEC has similar contribution to the power generation efficiencies as RC, but SEC is more complicated, which is not recommended. In summary, RC and SHC are two better bottom cycles for the hybrid cycle layout.

Main vapor temperatures elevating by increasing secondary air temperatures: Fig. 8 shows that the main vapor temperatures T_5 are elevated by increasing the secondary air temperatures $T_{sec\ air}$. For example, at $T_{sec\ air} = 330$ °C, T_5 covers the range of 570–670 °C with bottom cycle RC, and 550–650 °C with bottom cycle SHC. However, at $T_{sec\ air} = 430$ °C, the T_5 ranges are 660–700 °C adapting RC, and 620–700 °C adapting SHC. The temperature levels in which the top and bottom cycles operate are elevated by increasing $T_{sec\ air}$. The main vapor temperatures of top cycle should be raised to adapt such variation of $T_{sec\ air}$.

Power generation efficiencies weakly dependent on secondary air temperatures: There are two effects of $T_{sec\ air}$ on the hybrid cycle. The increase of $T_{sec\ air}$ increases extracted heat from flue gas by air preheater. The extracted heat is circulated from air preheater to furnace, which is a positive effect on the hybrid cycle. On the other hand, the rise of $T_{sec\ air}$ elevates CO_2 temperature entering heater 4 (T_{4b}), which should be adjusted by decreasing main vapor pressure of bottom cycle (P_{5b}). This is the negative effect which deteriorates thermal efficiency of bottom cycle. The comprehensive effect yields insensitive power generation efficiencies to the variation of secondary air temperatures.

Fig. 8e shows the thermal loads assigned to top cycle, bottom cycle and air preheater. $T_{sec\ air}$ does not influence the thermal load assigned to top cycle, but it balances the thermal loads applied to bottom cycle and air preheater. A lower $T_{sec\ air}$ increases thermal load applied to bottom cycle, but decreases thermal load applied to air preheater. At $T_{sec\ air} = 330$ °C and $T_5 = 700$ °C, the top cycle, bottom cycle and air preheater account for 72.79%, 13.40% and 13.82% of the total available flue gas energy, respectively.

For the hybrid cycle with RC, SRC or SHC as bottom cycle, the main vapor pressure of bottom cycle (P_{5b}) can be adjustable to have a wider secondary air temperature range to keep higher power generation efficiencies (see Fig. 8f). For coal fired power plant, the thermal load allocated to air preheater should not be large due to low heat transfer coefficients of flue gas and air. Usually, for supercritical water-steam power plant, $T_{sec\ air}$ is 330 °C, but it can be 400 °C maximumly [49]. The hybrid cycle not only keeps secondary air temperature in a similar level to that for supercritical water-steam cycle, but also has a power generation efficiency of about 51%, which is higher than supercritical water-steam cycle.

Fig. 9 shows the power generation efficiencies (η_e) dependent on pinch temperatures of CO_2 preheater PH ($\Delta T_{p,4}$) for hybrid cycle with

RC, SHC, PACC or SRC as bottom cycle. The parameters $T_{sec\ air} = 330\ ^{\circ}C$ and $T_{fg\ ex} = 123\ ^{\circ}C$ fixes the thermal load assigned to air preheater and specifies $T_{fg,o} = 390.10\ ^{\circ}C$. The equation of $T_{fg,o} = \Delta T_{p,4} + T_{4b} - 10$ indicates that with increase of $\Delta T_{p,4}$, the CO_2 temperature entering heater 4 (T_{4b}) is decreased, lowering CO_2 temperature levels in which top cycle and bottom cycle operate and degrading main vapor temperature regimes. For STB(RC) at $\Delta T_{p,4} = 30\ ^{\circ}C$, the T_5 range covers 590–680 °C, but the T_5 regime is shifted to 560–650 °C at $\Delta T_{p,4} = 50\ ^{\circ}C$.

We note that the sensitivity of effect of $\Delta T_{p,4}$ on system performance is different for different hybrid cycles (see Fig. 9). For STB(RC) and at $T_5 = 620\ ^{\circ}C$, when $\Delta T_{p,4}$ is varied in the range of 20–50 °C, P_{5b} should be adjusted in the range of 17.98–24.10 MPa to adapt pinch temperature variation, under which η_e is 47.95–47.96%, which is almost constant. On the other hand, STB(SHC) has an efficiency range of 48.03–47.93% for identical pinch temperature variation range, which is more sensitive than STB(RC). The sensitivity degree reflects the competition between pinch temperature of CO_2 preheater and main vapor pressure of bottom cycle. Our study shows that the hybrid cycles STB (RC), STB(SHC) and STB(PACC) are suitable for coal fired power plant with higher power generation efficiencies, in which top cycle uses RC + DRH and bottom cycles use RC, SHC or PACC, respectively (see Figs. 10–12). The heat transfer components are shown in Fig. 1b–d.

4.3. The outcome of connected-top-bottom-cycle (CTB)

CTB is expected to reach similar performance to STB but has simpler cycle layout. STB(RC) in Fig. 10 is converted to CTB(RC) in Fig. 13, and STB(SHC) in Fig. 11 is converted to CTB(SHC) in Fig. 14. CTB(RC) shown in Fig. 13a can operate with an FGC. In such a way, a smaller CO_2 flow rate is extracted from main compressor outlet of top cycle (C1), heated by FGC and then enters HTR2 of bottom cycle. CTB(RC) can also operate without FGC by by-passing CO_2 flow rate through FGC. Fig. 13b shows the *T*–*s* diagram with $P_5 = 30$ MPa, $T_5 = 665\ ^{\circ}C$, $T_{sec\ air} = 330\ ^{\circ}C$ and $\Delta T_{p,4} = 40\ ^{\circ}C$. The black and green colors represent top cycle and bottom cycle to show the energy cascade utilization. For top cycle, heaters 1, 2 and 3 deal with high temperature regime with CO_2 temperature range of 560.5–665.0 °C (see lines 4–5, 4′–5′ and 4″–5″). For bottom cycle, heater 4 deals with moderate temperature regime with CO_2 temperature range of 361.0–560.5 °C (see line 4b–5b). Having FGC in cycle, both air preheater and FGC recover low temperature flue gas heat. FGC deals with low temperature regime with CO_2 temperature range of 82.7–234.5 °C (see line 2–3). The recovery of flue gas heat by air preheater cannot be shown in *T*–*s* cycle.

Fig. 13c and d shows the linear relationship between power generation efficiencies and main vapor temperatures, showing the importance of T_5 on overall performance. We note that both CTB(RC) with and without FGC can successfully extract flue gas heat over entire temperature range. Comparing Fig. 13c and d identifies slightly higher power generation efficiencies without FGC than those with FGC. For example, at $T_5 = 700\ ^{\circ}C$, η_e is 51.21% without FGC, larger than the value of 50.75% with FGC. For CTB without FGC, the main vapor temperature range of 665–700 °C adapts the secondary air temperature range of 331.3–368.0 °C, indicating the adjustable function of air preheater to optimize thermal loads distribution among top cycle, bottom cycle and air preheater. For CTB with FGC, the split ratio x_{abs}, defined as mass flow rate extracted from main compressor outlet divided by total flow rate, behaves the adjustable function to optimize overall system performance. Based on our study, the connected cycle without FGC is recommended, not only possessing higher power generation efficiencies, but also creating acceptable secondary air temperatures.

Fig. 14 shows CTB(SHC) and calculation results. The bottom cycle SHC includes two heaters of 4a and 4b to recover moderate temperature flue gas heat. The two heaters are consecutively arranged in boiler flue tail. Fig. 14b shows the *T*–*s* diagram, including routes 4–5, 4′–5′ and 4″–5″ for high temperature flue gas heat extraction, and routes 3–4b′ and 4b–5b for moderate temperature flue gas heat extraction. The low temperature flue gas heat is extracted by FGC and air preheater. CTB (SHC) has similar relationships of parameters among η_e, x_{abs}, $T_{sec\ air}$ and T_5 to CTB(RC). We emphasize that, the main vapor temperature range of 620–700 °C for CTB(SHC) is wider than the range of 665–700 °C for CTB(RC).

Currently, the supercritical water-steam Rankine cycle power plant has main vapor parameters of 620 °C/30 MPa [32–34]. For S–CO_2 power plant using CTB(SHC) without FGC, the power generation efficiency is 47.92% at 620 °C/30 MPa, but it is increased to 51.21% at 700 °C/30 MPa. Once T_5 is elevated to 700 °C, P_5 can also be raised. Fig. 15 shows the increased power generation efficiencies versus main vapor pressures in the range of 26–40 MPa. Both CTB(RC) and CTB (SHC) share similar power generation efficiencies. The power efficiency is 51.82% at 700 °C/35 MPa, which is larger than existing power plant. CTB(RC) has lower secondary air temperatures than CTB(SHC). Among the two connected cycles, CTB(RC) and CTB(SHC) are suitable for higher and lower main vapor parameters, respectively.

5. Conclusions

Novel methods are developed to cascade utilize flue gas heat for coal fired power plant. Three kinds of cycles are proposed: RC + DRH + FGC, STB and CTB. Following conclusions can be drawn:

1. Even though RC + DRH + FGC keeps higher boiler efficiency and increases power generation efficiency compared with cycle without FGC, there exists power generation efficiency potential to be further explored.
2. For hybrid cycle construction, six bottom cycles are investigated, including our newly proposed bottom cycle SHC, which is suitable for wider main CO_2 vapor temperature range.
3. STB(RC), STB(SHC) and STB(PACC) have better comprehensive performance, adapting different main vapor temperature (T_5) ranges. At $T_{sec\ air} = 330\ ^{\circ}C$ and $\Delta T_{p,4} = 30\ ^{\circ}C$, the T_5 ranges are 550–590 °C for STB(SHC), 590–680 °C for STB(RC) and 680–700 °C for STB(PACC).
4. The parameter coordination principle is proposed to share specific components among top cycle and bottom cycle to form connected cycle, simplifying the system layout.
5. The connected cycle CTB(SHC) and CTB(RC) are suitable for main vapor temperature ranges of 620–665 °C and 665–700 °C, respectively. CTB(RC) has a power generation efficiency of 51.82% at main vapor parameters of 700 °C/35 MPa, significantly higher than available supercritical water-steam Rankine cycle power plant.

Acknowledgements

The study was supported by the National Key R&D Program of China (2017YFB0601801), the Fundamental Research Funds for the Central Universities (2018ZD02 and 2018QN042).

Appendix A

See Fig. A1.

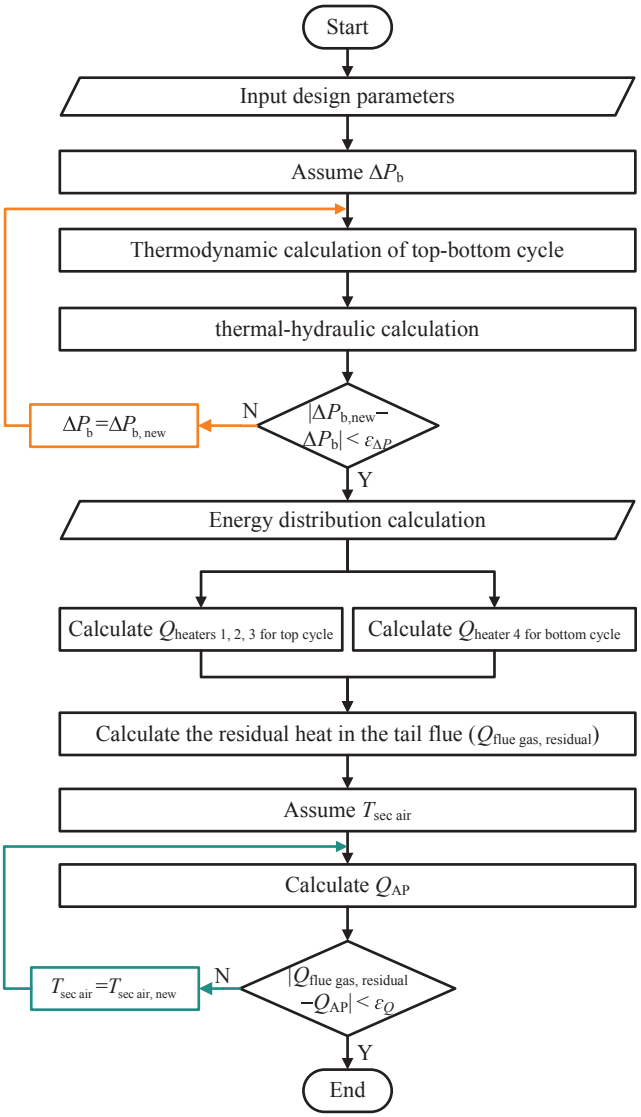

Fig. A1. Logic framework of the computation code.

References

[1] Parsons RH. The early days of the power station industry. Cambridge: Cambridge University Press; 2015.
[2] Tumanovskii AG, Shvarts AL, Somova EV, Verbovetskii EK, Avrutskii GD, Ermakova SV, et al. Review of the coal-fired, over-supercritical and ultra-supercritical steam power plants. Therm Eng 2017;64(2):83–96.
[3] Zhang NQ, Zhu ZL, Yue GQ, Jiang DF, Xu H. The oxidation behaviour of an austenitic steel in deaerated supercritical water at 600–700°C. Mater Charact 2017;132:119–25.
[4] Notton G, Nivet ML, Voyant C, Paoli C, Darras C, Motte F, et al. Intermittent and stochastic character of renewable energy sources: consequences, cost of intermittence and benefit of forecasting. Renew Sustain Energy Rev 2018;87:96–105.
[5] Merzic A, Music M, Haznadar Z. Conceptualizing sustainable development of conventional power systems in developing countries-A contribution towards low carbon future. Energy 2017;126:112–23.
[6] Yang YP, Wang LG, Dong CQ, Xu G, Morosuk T, Tsatsaronis G. Comprehensive exergy-based evaluation and parametric study of a coal-fired ultra-supercritical power plant. Appl Energy 2013;112:1087–99.
[7] Sonnenschein M, Lünsdorf O, Bremer J, Tröschel M. Decentralized control of units in smart grids for the support of renewable energy supply. Environ Impact Assess Rev 2015;52:40–52.
[8] Milani D, Luu MT, McNaughton R, Abbas A. Optimizing an advanced hybrid of solar-assisted supercritical CO_2 Brayton cycle: a vital transition for low-carbon power generation industry. Energy Convers Manage 2017;148:1317–31.
[9] Angelino G. Real gas effects in carbon dioxide cycles. In: ASME 1969 gas turbine conference and products show, Cleveland, OH.
[10] Holcomb GR, Carney C, Doğan ÖN. Oxidation of alloys for energy applications in supercritical CO_2 and H_2O. Corros Sci 2016;109:22–35.
[11] Dostal V. A supercritical carbon dioxide cycle for next generation nuclear reactors. PhD thesis, Nuclear Engineering, Massachusetts Institute of Technology; 2004.
[12] Lv G, Yang J, Shao W, Wang X. Aerodynamic design optimization of radial-inflow turbine in supercritical CO_2 cycles using a one-dimensional model. Energy Convers Manage 2018;165:827–39.
[13] Sulzer G. Verfahren zur Erzeugung von Arbeit aus Warme. Swiss Patent. 1950;269599.
[14] Feher EG. The supercritical thermodynamic power cycle. Energy Convers Manage 1968;8:85–90.
[15] Moisseytsev A, Sienicki JJ. Investigation of alternative layouts for the supercritical carbon dioxide Brayton cycle for a sodium-cooled fast reactor. Nucl Eng Des 2009;239:1362–71.
[16] Ahn Y, Lee JI. Study of various Brayton cycle designs for small modular sodium-cooled fast reactor. Nucl Eng Des 2014;276:128–41.

[17] Cheng W, Huang W, Nian Y. Global parameter optimization and criterion formula of supercritical carbon dioxide Brayton cycle with recompression. Energy Convers Manage 2017;150:669–77.
[18] Kouta A, Al-Sulaiman F, Atif M, Marshad SB. Entropy, exergy, and cost analyses of solar driven cogeneration systems using supercritical CO_2 Brayton cycles and MEE-TVC desalination system. Energy Convers Manage 2016;115:253–64.
[19] Wang X, Liu Q, Lei J, Han W, Jin H. Investigation of thermodynamic performances for two-stage recompression supercritical CO_2 Brayton cycle with high temperature thermal energy storage system. Energy Convers Manage 2018;165:477–87.
[20] Ehsan MM, Guan Z, Klimenko AY, Wang X. Design and comparison of direct and indirect cooling system for 25 MW solar power plant operated with supercritical CO_2 cycle. Energy Convers Manage 2018;168:611–28.
[21] Kim MS, Ahn Y, Kim B, Lee JI. Study on the supercritical CO_2 power cycles for landfill gas firing gas turbine bottoming cycle. Energy 2016;111:893–909.
[22] Kim YM, Sohn JL, Yoon ES. Supercritical CO_2 Rankine cycles for waste heat recovery from gas turbine. Energy 2017;118:893–905.
[23] Hou S, Zhou Y, Yu L, Zhang F, Cao S. Optimization of the combined supercritical CO_2 cycle and organic Rankine cycle using zeotropic mixtures for gas turbine waste heat recovery. Energy Convers Manage 2018;160:313–25.
[24] Heo JY, Kim MS, Baik S, Bae SJ, Lee JI. Thermodynamic study of supercritical CO_2 Brayton cycle using an isothermal compressor. Appl Energy 2017;206:1118–30.
[25] Liu M, Zhang X, Ma Y, Yan J. Thermo-economic analyses on a new conceptual system of waste heat recovery integrated with an S-CO_2 cycle for coal-fired power plants. Energy Convers Manage 2018;161:243–53.
[26] Besarati SM, Goswami DY, Stefanakos EK. Development of a solar receiver based on compact heat exchanger technology for supercritical carbon dioxide power cycles. J Sol Energy Eng 2015;137(3):31018.
[27] Xu RN, Luo F, Jiang PX. Buoyancy effects on turbulent heat transfer of supercritical CO_2 in a vertical mini-tube based on continuous wall temperature measurements. Int J Heat Mass Transf 2017;110:576–86.
[28] Son S, Heo JY, Lee JI. Prediction of inner pinch for supercritical CO_2 heat exchanger using Artificial Neural Network and evaluation of its impact on cycle design. Energy Convers Manage 2018;163:66–73.
[29] Pasch J, Carlson M, Fleming D, Rochau G. Evaluation of recent data from the SANDIA national laboratories closed Brayton cycle testing. In: ASME, editor. Proceeding of ASME turbo expo 2016: turbomachinery technical conference and exposition, Seoul.
[30] Clementoni EM, Cox TL, King MA. Off-nominal component performance in a supercritical carbon dioxide Brayton cycle. J Eng Gas Turb Power 2016;138:011703.
[31] Iverson BD, Conboy TM, Pasch JJ, Kruizenga AM. Supercritical CO_2 Brayton cycles for solar-thermal energy. Appl Energy 2013;111:957–70.
[32] Le Moullec Y. Conceptual study of a high efficiency coal-fired power plant with CO_2 capture using a supercritical CO_2 Brayton cycle. Energy 2013;49:32–46.
[33] Mecheri M, Le Moullec Y. Supercritical CO_2 Brayton cycles for coal-fired power plants. Energy 2016;103:758–71.
[34] Hanak DP, Manovic V. Calcium looping with supercritical CO_2 cycle for decarbonisation of coal-fired power plant. Energy 2016;102:343–53.
[35] Chen S, Soomro A, Yu R, Hu J, Sun Z, Xiang W. Integration of chemical looping combustion and supercritical CO_2 cycle for combined heat and power generation with CO_2 capture. Energy Convers Manage 2018;167:113–24.
[36] Johnson GA, McDowell MW, O'Connor GM, Sonwane CG, Subbaraman G. Supercritical CO2 cycle development at Pratt & Whitney Rocketdyne. In: ASME turbo expo 2012:turbine technical conference and exposition. No. GT2012-70105; 2012.
[37] Basu P, Kefa C, Jestin L. Boilers and burners: design and theory. New York: Springer Science & Business Media; 2012.
[38] Bai ZW, Zhang GQ, Li YY, Xu G, Yang YP. A supercritical CO_2 Brayton cycle with a bleeding anabranch used in coal-fired power plants. Energy 2018;142:731–8.
[39] Park SH, Kim JY, Yoon MK, Rhim DR, Yeom CS. Thermodynamic and economic investigation of coal-fired power plant combined with various supercritical CO_2 Brayton power cycle. Appl Therm Eng 2018;130:611–23.
[40] Yang Y, Bai WG, Wang YM, Zhang YF, Li HZ, Yao MY, et al. Coupled simulation of the combustion and fluid heating of a 300MW supercritical CO_2 boiler. Appl Therm Eng 2017;113:259–67.
[41] Sarkar J. Second law analysis of supercritical CO_2 recompression Brayton cycle. Energy 2009;34:1172–8.
[42] Turchi CS, Ma ZW, Neises TW, Wagner MJ. Thermodynamic study of advanced supercritical carbon dioxide power cycles for concentrating solar power systems. J Sol Energy Eng 2013;135(4):41007.
[43] Li MJ, Zhu HH, Guo JQ, Wang K, Tao WQ. The development technology and applications of supercritical CO_2 power cycle in nuclear energy, solar energy and other energy industries. Appl Therm Eng 2017;126:255–75.
[44] Wang K, He YL, Zhu HH. Integration between supercritical CO_2 Brayton cycles and molten salt solar power towers: a review and a comprehensive comparison of different cycle layouts. Appl Energy 2017;195:819–36.
[45] Lemmon EW, Huber ML, Mc Linden MO. NIST standard reference database 23: reference fluid thermodynamic and transport properties-REFPROP, version 9.1. Tech. rep. Gaithersburg: National Institute of Standards and Technology, Standard Reference Data Program; 2013.
[46] Padilla RV, Too YCS, Benito R, Stein W. Exergetic analysis of supercritical CO_2 Brayton cycles integrated with solar central receivers. Appl Energy 2015;148:348–65.
[47] Liu ZB, He YL, Yang YF, Fei JY. Experimental study on heat transfer and pressure drop of supercritical CO_2 cooled in a large tube. Appl Therm Eng 2014;70:307–15.
[48] Zhou LY, Xu G, Zhao SF, Xu C, Yang YP. Parametric analysis and process optimization of steam cycle in double reheat ultra-supercritical power plants. Appl Therm Eng 2016;99:652–60.
[49] Wang LM, Deng L, Tang CL, Fan Q, Wang CX, Che DF. Thermal deformation prediction based on the temperature distribution of the rotor in rotary air-preheater. Appl Therm Eng 2015;90:478–88.